Article

Molecular Cell

Targeted Enhancer Activation by a Subunit of the Integrator Complex

Graphical Abstract

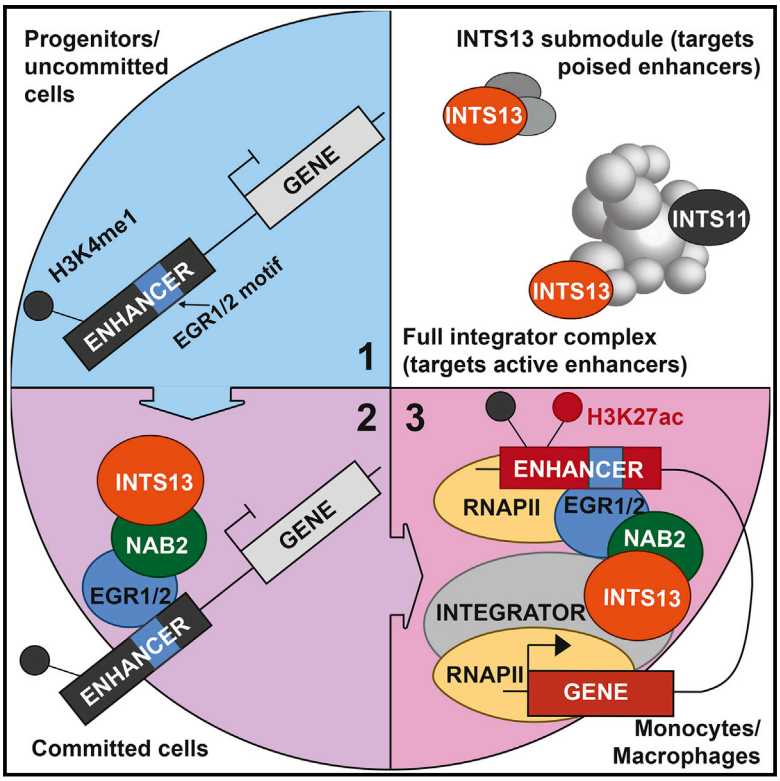

Highlights

- INTS13 is a modular subunit of Integrator dispensable for the catalytic activity
- INTS13 is non-essential in progenitor cells but required for monocytic commitment
- The co-factor NAB2 drives INTS13 to poised EGR1 enhancers
- INTS13 mediates activation of monocytic enhancers

Authors

Elisa Barbieri, Marco Trizzino, Sarah Ann Welsh, ..., Martin Carroll, Kavitha Sarma, Alessandro Gardini

Correspondence

agardini@wistar.org

In Brief

Barbieri et al. demonstrate that a subunit of the Integrator complex, INTS13, is required for monocytic commitment of myeloid progenitors. INTS13 is a modular component of Integrator recruited to poised enhancers via the EGR1 transcription factor and its co-factor NAB2. The INTS13/EGR1/NAB2 axis is essential to elicit enhancer-mediated gene activation.

Barbieri et al., 2018, Molecular Cell *71*, 103–116
July 5, 2018
https://doi.org/10.1016/j.molcel.2018.05.031

CellPress

Molecular Cell
Article

Targeted Enhancer Activation by a Subunit of the Integrator Complex

Elisa Barbieri,[1,5] Marco Trizzino,[1,5] Sarah Ann Welsh,[1,2] Tori Alexandra Owens,[1] Bruno Calabretta,[3] Martin Carroll,[4] Kavitha Sarma,[1] and Alessandro Gardini[1,6,*]
[1]The Wistar Institute, Gene Expression and Regulation Program, 3601 Spruce Street, Philadelphia, PA 19104, USA
[2]Biochemistry and Molecular Biophysics Graduate Group, Perelman School of Medicine, University of Pennsylvania, 3400 Civic Center Boulevard, Philadelphia, PA 19104, USA
[3]Sidney Kimmel Cancer Center, Thomas Jefferson Medical School, Philadelphia, PA, USA
[4]Division of Hematology and Oncology, University of Pennsylvania, Philadelphia, PA, USA
[5]These authors contributed equally
[6]Lead Contact
*Correspondence: agardini@wistar.org
https://doi.org/10.1016/j.molcel.2018.05.031

SUMMARY

The control of cell fate is an epigenetic process initiated by transcription factors (TFs) that recognize DNA motifs and recruit activator complexes and transcriptional machineries to chromatin. Lineage specificity is thought to be provided solely by TF-motif pairing, while the recruited activators are passive. Here, we show that INTS13, a subunit of the Integrator complex, operates as monocytic/macrophagic differentiation factor. Integrator is a general activator of transcription at coding genes and is required for eRNA maturation. Here, we show that INTS13 functions as an independent sub-module and targets enhancers through Early Growth Response (EGR1/2) TFs and their co-factor NAB2. INTS13 binds poised monocytic enhancers eliciting chromatin looping and activation. Independent depletion of INTS13, EGR1, or NAB2 impairs monocytic differentiation of cell lines and primary human progenitors. Our data demonstrate that Integrator is not functionally homogeneous and has TF-specific regulatory potential, revealing a new enhancer regulatory axis that controls myeloid differentiation.

INTRODUCTION

Cis-regulatory elements orchestrate spatial and temporal gene expression in metazoans. Enhancers are essential during tissue development and cell differentiation, such as in the hematopoietic compartment (Álvarez-Errico et al., 2015; Heinz et al., 2015; Huang et al., 2016). Precisely, recognition of DNA motifs by a select combination of transcription factors (TFs) activates enhancers that were otherwise repressed or in a poised/inactive conformation (Heinz et al., 2010, 2015). While repressed enhancers lack DNA accessibility and are embedded in a repressive chromatin conformation, poised enhancers are generally nucleosome-free to facilitate binding of lineage-determining TFs to their respective DNA motifs. Poised enhancers are devoid of H3K27ac mark (enriched at enhancers that are active or recently dismissed) but carry sustained levels of H3K4me1 (Creyghton et al., 2010; Rada-Iglesias et al., 2011). It is believed that recruitment of TFs first leads to hyper-acetylation of nucleosomes surrounding the enhancer core (Whyte et al., 2013). Next, TFs pair with the Mediator complex to recruit the RNAPII holoenzyme and initiate bi-directional transcription of enhancer-associated noncoding RNAs (eRNAs) (Li et al., 2013). The Integrator, a large co-activator complex endowed with RNA endonucleolytic activity, is required to terminate eRNA transcripts and consequently allow their accumulation at chromatin. eRNAs are implicated in enhancer activation, perhaps by enforcing chromosomal looping between enhancers and their target promoters (Hsieh et al., 2014; Lai et al., 2015). In addition, eRNAs may function in maintenance of H3K27ac levels (Bose et al., 2017), and in release of the paused RNAPII at target promoters (Schaukowitch et al., 2014). The overall mechanistic process of enhancer activation is not clear. For instance, the series of events that bring inactive or poised enhancers to full activation is poorly understood. Here, we present a novel function for a component of the Integrator complex in activating lineage-specific enhancers.

Integrator is conserved across metazoans and is composed of 14 subunits (INTS1–INTS14) (Baillat et al., 2005; Chen et al., 2012). This protein complex associates with the C-terminal domain of RNAPII and is implicated in the biogenesis of spliceosomal U small nuclear RNAs (snRNAs) (Baillat et al., 2005). In fact, the endonucleolytic heterodimer INTS9/INTS11 cleaves nascent U snRNA transcripts to initiate their maturation (Baillat et al., 2005). Integrator's activity at enhancers is also critical to establish chromosomal looping with target promoters to drive gene activation (Lai et al., 2015). Furthermore, Integrator is loaded at the proximal promoter of protein-coding genes, where it controls the release of paused RNAPII by recruiting the SEC/pTEFb complex and modulating the activity of Negative Elongation Factor (NELF) (Gardini et al., 2014; Stadelmayer et al., 2014). While the catalytic function and genomic distribution of the INTS9/INTS11 heterodimer has been established, the remaining

12 subunits of the complex are largely uncharacterized. Here, we describe that the INTS13 subunit has a lineage-specific role in regulating enhancer activity. Our data indicate that INTS13 regulates enhancer regions bound by the EGR1/2 TFs, in association with the co-factor NAB2, during differentiation of progenitor cells into monocytes and macrophages.

In the myeloid branch of hematopoiesis, monocytes and macrophages (the tissue-resident counterpart of monocytes) are specialized phagocytic cells that rely on TFs such as SPI1, CEBPα, and CEBPβ as master determinants of commitment and differentiation (Álvarez-Errico et al., 2015; Friedman, 2007; Scott et al., 1994). Some of these TFs, such as SPI1, are also critical in regulating the activity of terminally differentiated macrophages (Barozzi et al., 2014; Heinz et al., 2010; Ostuni et al., 2013). While the Early Growth Response (EGR) TFs have largely been studied during neural development (Giudicelli et al., 2001; Poirier et al., 2008; Thierion et al., 2017), EGR1/2 are also active during myelopoiesis, promoting monocytic/macrophagic differentiation in a variety of human cell lines as well as primary myeloid precursors (Krishnaraju et al., 2001; Laslo et al., 2006; Nguyen et al., 1993; Pham et al., 2012). Our data support a fundamental role for EGR1/2 in monocytic commitment and defines their activity at critical lineage-determining enhancers, such as the enhancer of *CSF1R*. Furthermore, we identify NAB2, previously suggested to be a repressor of EGR1 activity (Kumbrink et al., 2010), as the fundamental co-activator of monocytic enhancers in association with EGR1 and the Integrator complex. In summary, we describe a network of enhancers driving differentiation via the Integrator/EGR/NAB2 axis and provide the first evidence that Integrator has modular components, conferring lineage-specific activity to this evolutionarily conserved complex.

RESULTS

Functional Dissection of the INTS11 and INTS13 Subunits of Integrator

Integrator targets active protein-coding genes, regulates the release of paused RNAPII from proximal promoters (Gardini et al., 2014; Stadelmayer et al., 2014; van den Berg et al., 2017), and modulates the biogenesis of noncoding eRNAs at enhancers through the endonucleolytic activity of the INTS11 subunit (Lai et al., 2015). Unlike Mediator, Integrator is specific to metazoans, suggesting that it may play a role in tissue and cell-fate specification. To dissect the role of Integrator in gene regulation, we examined the poorly characterized INTS13 subunit, along with the core catalytic subunit INTS11, in the myeloid HL-60 cell line.

First, we immunoprecipitated INTS13 from the nuclear extract of HL-60 cells and found strong association with INTS11 and INTS1, indicating that INTS13 is a bona fide component of Integrator in myeloid cells (Figures 1A and 1B). Second, to begin characterizing the role of INTS13 within the Integrator complex, we assayed RNA endonucleolytic activity by qRT-PCR. We depleted INTS13 and INTS11 in HL-60 cells and measured accumulation of primary unprocessed U1 snRNA transcript. In the absence of INTS13, the basal catalytic activity of the Integrator complex was not affected (Figures 1C, S1A, and S1B). Additionally, we found that INTS13 is dispensable for proliferation of HL-60 myeloid progenitor cells, whereas depletion of INTS11, predictably, suppresses cell growth (Figure 1D). These data suggest that INTS13 is not essential for the fitness of HL-60 cells and may have a very limited function within the Integrator complex in this cell model.

Next, we assessed whether the Integrator subunits were required for gene activation associated to monocytic differentiation of HL-60. HL-60 are progenitor-like cells of myeloid origin (established from a patient with promyelocytic leukemia) (Gallagher et al., 1979) that can be differentiated into functional monocytes/macrophages upon stimulation with PMA (phorbol myristate acetate), providing a convenient model of differentiation. We examined the induction of the prototypical monocytic gene *CSF1R*, which encodes the membrane receptor for the monocytic cytokine macrophage colony-stimulating factor (M-CSF) and is specifically induced during differentiation and found that INTS11 is necessary for induction of *CSF1R* (Figure 1E), similar to its requirement for activation of immediate early genes by the epidermal growth factor (Gardini et al., 2014; Lai et al., 2015). Surprisingly, we also found INTS13 to be required for induction of *CSF1R* (40%–70% reduction of expression with small hairpin RNAs [shRNAs] for INTS13, Figures 1E and S1A for knockdown efficiency) suggesting that this subunit, while dispensable in progenitor cells, may be necessary for differentiation. We treated HL-60 cells with PMA for 48 hr and measured expression of the surface marker CD11b by fluorescence-activated cell sorting (FACS) analysis (Bender and Beavo, 2006). Depletion of INTS13 with two different shRNAs resulted in significant decrease of CD11b (Figures 1F and S1A). To ensure that the effect of INTS13 on monocytic differentiation is physiologically relevant and not dependent on HL-60 cells and PMA stimulation, we purified $CD34^+$ stem and progenitor cells from cord blood. First, we assessed proliferation of primary cells after depletion of INTS11 and INTS13 by measuring their metabolic activity (MTT assay at day 4 post puromycin selection). Similar to HL-60, only INTS11 depletion affected the growth of primary progenitor cells (Figures 1G and S1B). Next, we leveraged INTS13-depleted $CD34^+$ cells in a colony forming unit (CFU) assay to assess their potential to form monocytic/macrophagic colonies in semi-solid medium upon stimulation with M-CSF and granulocyte-macrophage (GM)-CSF for 2 weeks. Our data indicated that INTS13 is required, in primary human cells, to form monocytic colonies (Figures 1H, S1B, and S1C) and suggest that INTS13 has a specific role in determining the monocytic fate of progenitor cells.

The INTS13 Subunit of Integrator Is Required for Activation of the Monocytic Transcriptome

We analyzed the transcriptome of HL-60 cells before and after 16 hr of PMA induction using RNA sequencing (RNA-seq). PMA stimulation resulted in differential expression of 842 genes (DESeq2, false discovery rate [FDR] <5%). Notably, the majority (75%) of genes were upregulated (Figure 2A) and highly enriched in gene ontology categories related to immune cell differentiation and cellular movement, the latter being a feature of differentiated macrophages (Figure S2A). In sum, a short treatment of PMA triggered robust induction of genes that confer

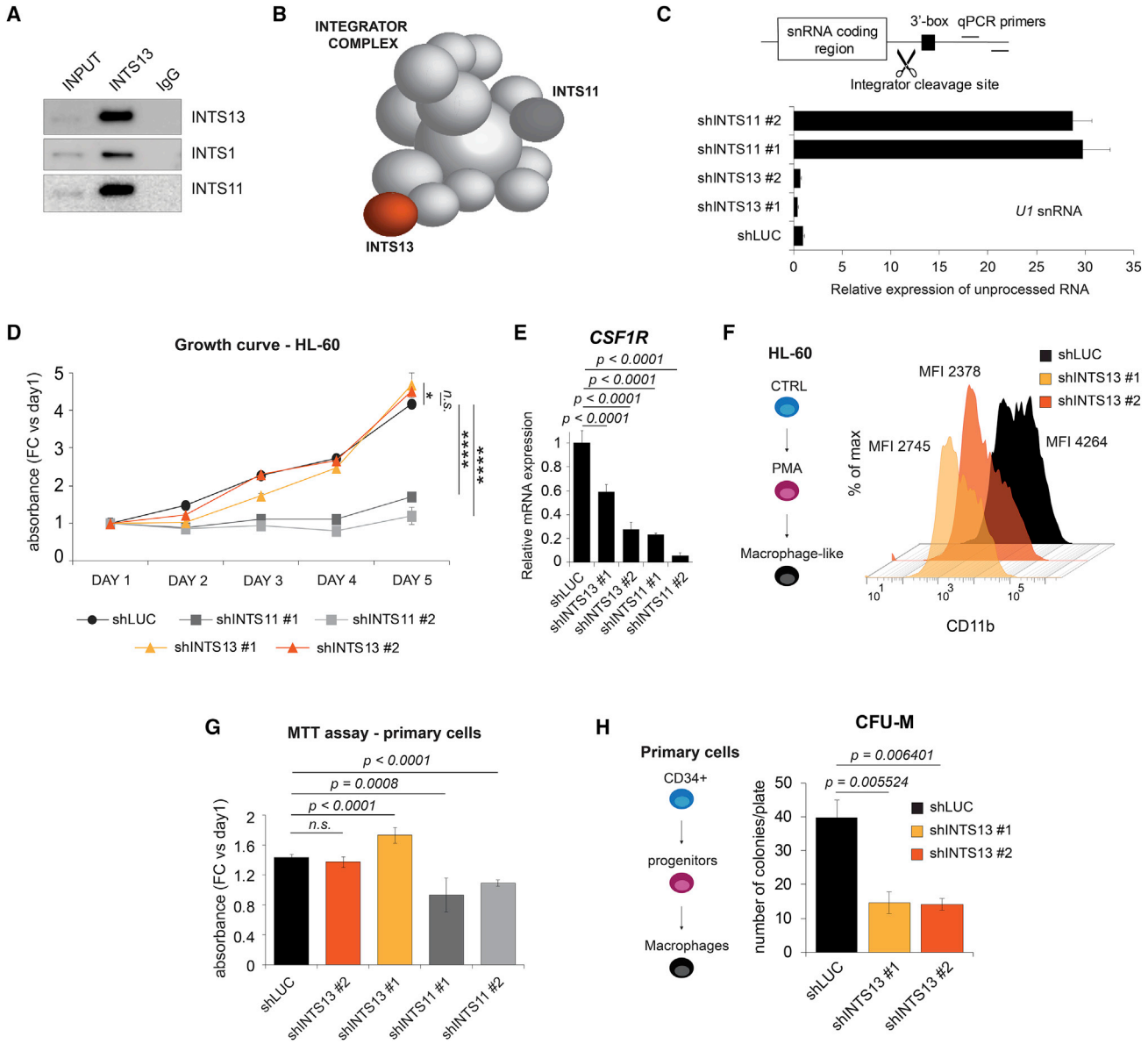

Figure 1. Functional Dissection of the INTS11 and INTS13 Subunits of Integrator

(A) Immunoprecipitation of INTS13 in HL-60 cells. Immunoblots of antibodies against the Integrator subunits INTS1 and INTS11 show that the complex co-precipitates with INTS13.

(B) Model representation of the Integrator protein complex, including the subunits INTS11 and INTS13.

(C) qRT-PCR of *U1* snRNA in untreated HL-60 transduced with two different shRNAs against INTS11 and INTS13 shows that INTS11 depletion abrogates the catalytic activity of the complex while it is maintained upon INTS13 knockdown. Primers were designed downstream to the core snRNA sequence, after the region recognized and cleaved by Integrator. shRNAs against luciferase (shLUC) were used as a control and ribosomal *18S* as housekeeping gene. Data are means ± SD.

(D) Five-day growth curve (MTT assay based) of unstimulated HL-60 cells transduced with shRNAs against INST11 and INTS13. Depletion of INTS13 does not impair proliferation of HL-60, whereas depletion of INTS11 results in strong growth suppression. Two shRNAs per subunit were employed. Data are means ± SD.

(E) qRT-PCR of the monocytic gene *CSF1R* in PMA-treated HL-60 following depletion of either INTS11 or INTS13. Depletion of both INTS13 and INTS11 negatively affects *CSF1R* activation by PMA.

(F) HL-60 cells treated with PMA differentiate into a macrophagic-like stage and expression of the surface integrin CD11b is a measure of differentiation. The mean fluorescence intensity (MFI) of CD11b decreases in differentiated cells after depletion of INTS13 with two different shRNAs (48 hr post-PMA induction).

(G) Metabolic activity assay (MTT) was performed on $CD34^+$ cells transduced with shRNAs for INTS11 and INTS13; data were collected at day 1 and day 4 after selection with puromycin and plotted as fold change (FC; day 4 versus day 1). The MTT shows that also in primary cells the depletion of INTS13 does not impair proliferation, whereas depletion of INTS11 results in strong growth suppression. Data are means ± SD.

(H) Colony-forming unit (CFU) assay of cord-blood-derived $CD34^+$ cells infected with two different shRNAs for INTS13 and induced by M-CSF in methylcellulose medium. The number of monocytic/macrophagic CFUs is significantly reduced in INTS13-depleted cells compared to control (shLUC). Data are means ± SD.

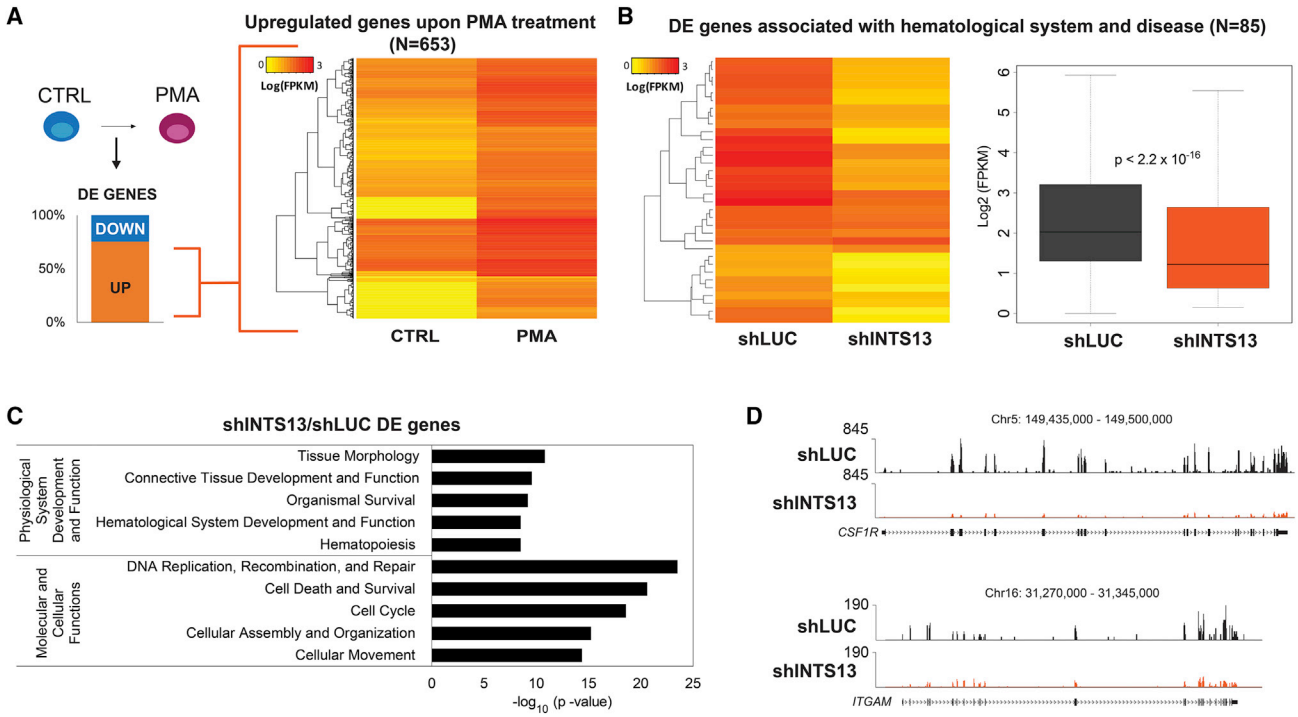

Figure 2. Depletion of INTS13 Affects the Expression of Monocyte-Specific Genes

(A) 842 genes are DE between differentiated (PMA) and undifferentiated (CTRL) HL-60 cells (FDR <5%): 653 upregulated, 189 downregulated. The heatmap displays the change in expression for the 653 upregulated genes.

(B) Heatmap and box plot show that the depletion of INTS13 in PMA treated HL-60 significantly decreases expression of genes associated to hematological system and diseases.

(C) Ingenuity pathway analysis on 974 genes detected as DE in INTS13-depleted cells (FDR <5%) reveals enrichment for hematopoiesis related processes.

(D) Screenshots of the monocytic genes *CSF1R* and *ITGAM*, whose expression is strongly decreased upon INTS13 depletion in PMA-stimulated HL-60 cells.

monocytic/macrophagic identity in HL-60 cells (similar to primary cells after a short treatment with M-CSF in liquid culture, see Figures S2B and S2C). Next, we depleted INTS13 in HL-60 cells using lentiviral-transduced shRNAs. We found 974 genes differentially expressed (2 independent replicates, fold change > ± 2, FDR <5%) with respect to control (shLUC). The genes differentially expressed (DE) were enriched for hematopoiesis and immune cell development, as revealed by pathway analysis (Figure 2C). Notably, we observed that monocytic/macrophagic genes were not properly activated in the absence of INTS13 (Figures 2B, S2D, and S2E). Among DE genes were *CSF1R* (surface receptor for M-CSF) and *ITGAM* (part of the monocytic adhesion molecule CD11b) (Figure 2D). Taken together, our data suggest that INTS13 is critical for the timely activation of monocytic genes and is essential to coordinate transcriptome changes that define the monocytic/macrophagic lineage.

Modular Properties of the Integrator Complex during Differentiation of Myeloid Cells

To define the activity of the Integrator complex during lineage commitment and differentiation of monocytes/macrophages, we generated chromatin immunoprecipitation sequencing (ChIP-seq) profiles before and after differentiation induced by PMA (Figure 3A), to determine whether the dynamics of INTS11 and INTS13 binding at chromatin could explain their different roles in progenitors and monocytes. Our ChIP-seq analysis retrieved comparable numbers of binding sites for the two subunits: 11,418 replicated peaks for INTS11-CTRL, 14,337 for INTS11-PMA, 14,408 for INTS13-CTRL, and 15,966 for INTS13-PMA (Table S4).

To focus on the changes in Integrator binding upon differentiation, we independently performed differential binding analysis (CTRL versus PMA) using edgeR for each of the two subunits (Robinson et al., 2010; FDR <10%, Table S1). With this analysis, we detected 5,728 regions that significantly gained INTS13 binding upon differentiation (hereafter INTS13-gained regions; Figure 3B), and 2,438 regions with significant increase in INTS11 (hereafter INTS11-gained regions; Figure 3B). Notably, INTS11-gained regions were largely enriched for proximal promoters (62.2%), mirroring the known RNAPII-associated activity of the complex, and displayed robust binding of INTS13 as well (Figures 3B and 3C). Conversely, INTS13-gained regions were largely found distal from the TSS of protein-coding genes (82.5%) and only partially overlapped with INTS11 (Figures 3B and 3D).

We further investigated whether isolated INTS13-gained regions could simply be the result of differences in pull-down efficiency. First, we profiled INTS11 and INTS13 at all active U snRNA genes (due to their high rate of transcription, U snRNA

loci bear the highest amount of the Integrator complex) and found INTS11 to be more abundant than INTS13, suggesting that the INTS11 antibody performs well in ChIP-seq (Figure 3E). Next, we validated our findings by quantitative ChIP at select loci. While INTS13 and INTS11 were recovered at similar levels at the transcription start site of genes such as *FOS* and *JUN* (Figures 3F and S3), only INTS13 was significantly detected at intergenic loci for which ChIP-seq revealed isolated binding (Figures 3F and S3). INTS1 and INTS6, additional subunits of the full Integrator complex, were also absent from INTS13-specific sites (Figures 3F and S3). To investigate the modularity of the Integrator complex *in vivo*, we subjected nuclear extract of HL-60 cells to fractionation on a size-exclusion column (Superose 6). Notably, INTS13—along with other Integrator subunits (INTS1, INTS6, INTS11)—elutes at a large molecular weight (>2 MDa), comprising the full Integrator complex and associated RNAPII, as previously described (Baillat et al., 2005). However, we observed a second elution peak of INTS13, centered around fraction 38 (~200 kDa), which suggests the existence of INTS13 as a sub-module (Figure 3G). To ensure that the smaller INTS13 module is biochemically distinct from the previously described INTS9/INTS11 heterodimer (Baillat et al., 2005; Albrecht and Wagner, 2012), we performed immunoprecipitation of INTS13 from fraction 38 and subjected the eluate to LC-MS/MS. Besides INTS13, we retrieved peptides of INTS14 and INTS10 and no peptides of INTS11 (Figure S3). Together, our data demonstrate that INTS13 may also exist as a separate module in the nucleoplasm, perhaps associated with additional Integrator subunits and may be selectively recruited to genomic sites during monocytic differentiation, even in the absence of the full Integrator complex.

INTS13 Binds to Monocytic Enhancers during Differentiation

To understand the lineage-specific role of INTS13, we examined the regions where it was recruited to chromatin upon differentiation (5,728 INTS13-gained regions, Figure 3B). Topological analysis suggested that the large majority of INTS13-gained sites (82.5% = 4,274 sites) were distal from the TSS of protein-coding genes (Figure 3B). We identified the nearest genes for all the distal regions, based on distance from TSS, and examined gene ontology categories. We found that, collectively, INTS13-gained distal regions were significantly associated with genes implicated in immune cell development, trafficking, and hematopoiesis (Data S1). We hypothesized that these distal regions could be enhancers, and we characterized them by performing H3K27ac, H3K4me1, and total RNAPII ChIP-seq in HL-60 cells, both untreated and upon 16 hr of PMA stimulation. We specifically examined the status of acetylation and methylation at INTS13-gained distal regions and found that ~90% of these regions overlap a peak of H3K4me1, but only ~50% also overlap a peak of H3K27ac, supporting two distinct categories of INTS13-bound enhancers (Figure 4A). The first category (representing ~50% of all enhancers) comprised active enhancers with high H3K27ac, RNAPII, and INTS11 (Figures 4A and 4B). In particular, the intronic enhancer of *CSF1R*, also known as the FIRE element (Himes et al., 2001; Krysinska et al., 2007), was active and significantly enriched for INTS13 (Figure 4B). Notably, these enhancers boast transcription of eRNAs, underscoring their active status (Figure S4). The second category of INTS13-bound enhancers was enriched in H3K4me1, but lacked RNAPII and INTS11, and displayed low or undetectable H3K27ac (Figures 4A and 4B). These data suggested that INTS13 can also be recruited to enhancers that are poised (Figure 4B). Therefore, we speculated that INTS13 might be recruited to the active monocytic enhancers at earlier time points of PMA induction, when the enhancers are still in a poised/inactive state. Consistently, time-course analysis of PMA induction suggested that binding of INTS13 precedes activation of the enhancer as measured by increase in acetylation of H3K27 (Figure 4C). In particular, the enhancer of *CSF1R* displays an ~25-fold increase of INTS13 at 4 hr post-induction, whereas the surge of H3K27ac (~18-fold) was detected at 6 hr. On the other hand, poised enhancers bound by INTS13 at 16 hr of PMA treatment may be activated at later time points, as suggested by our ChIP-seq analysis of an extended time course of H3K27ac (Figure 4D).

In summary, we demonstrated that the INTS13 subunit of Integrator selectively binds monocytic enhancers during lineage-specific differentiation. INTS13 is recruited to enhancers before acetylation of H3K27 and is likely to play a role in the enhancer activation process.

INTS13 Targets EGR-Responsive Sites Genome-wide

The Integrator complex is believed to be recruited at chromatin through its well-established interaction with the carboxy-terminal domain (CTD) of RNAPII (Baillat et al., 2005; Egloff et al., 2010). Our data suggested, for the first time, that a component of Integrator is recruited at chromatin independently of the rest of the complex and in the absence of RNAPII. Specifically, we have established that INTS13 targets poised enhancer sites, which are deprived of RNAPII and INTS11. We surmised that a TF may be implicated in the recruitment of INTS13, whose protein sequence lacks any recognizable DNA/chromatin binding domain. Therefore, we performed *de novo* motif analysis on the 4,274 INTS13-gained enhancers enriched during differentiation (see Figure 4A). We identified a matrix for the EGR1/EGR2 TFs as the most significant hit of the motif analysis (Figure 5A). While other myeloid TF motifs were also retrieved (i.e. SPI1, ERG/Ets, AP-1), their relative abundance and their significance lag well behind that of EGR1/2 (see Data S2). Importantly, the EGR1/2 motif was centrally enriched, further underscoring its association with INTS13. We tested the possibility that association with INTS13 and EGR1 sites may be a conserved feature in different model systems. We treated Jurkat lymphoblastic T cells with PMA to mimic T cell activation and assessed the distribution of INTS13. Notably activation of Jurkat cells resulted in *de novo* binding of INTS13 to 1,026 EGR1 sites, distinct from the monocytic ones, which appeared to be enhancers associated with T cell activity (Figures S5A–S5F; motif and ingenuity pathway analysis (IPA) pathways analyses in Data S3).

The Early Growth Factor 1 and 2 are paralog genes that encode zinc finger TFs widely implicated in cell growth and differentiation. Importantly, EGR1 determines monocytic/macrophagic differentiation when expressed in primary and stable cell lines, similar to EGR2 (Laslo et al., 2006; Nguyen et al., 1993). We performed ChIP-seq for EGR1 in HL-60 cells and

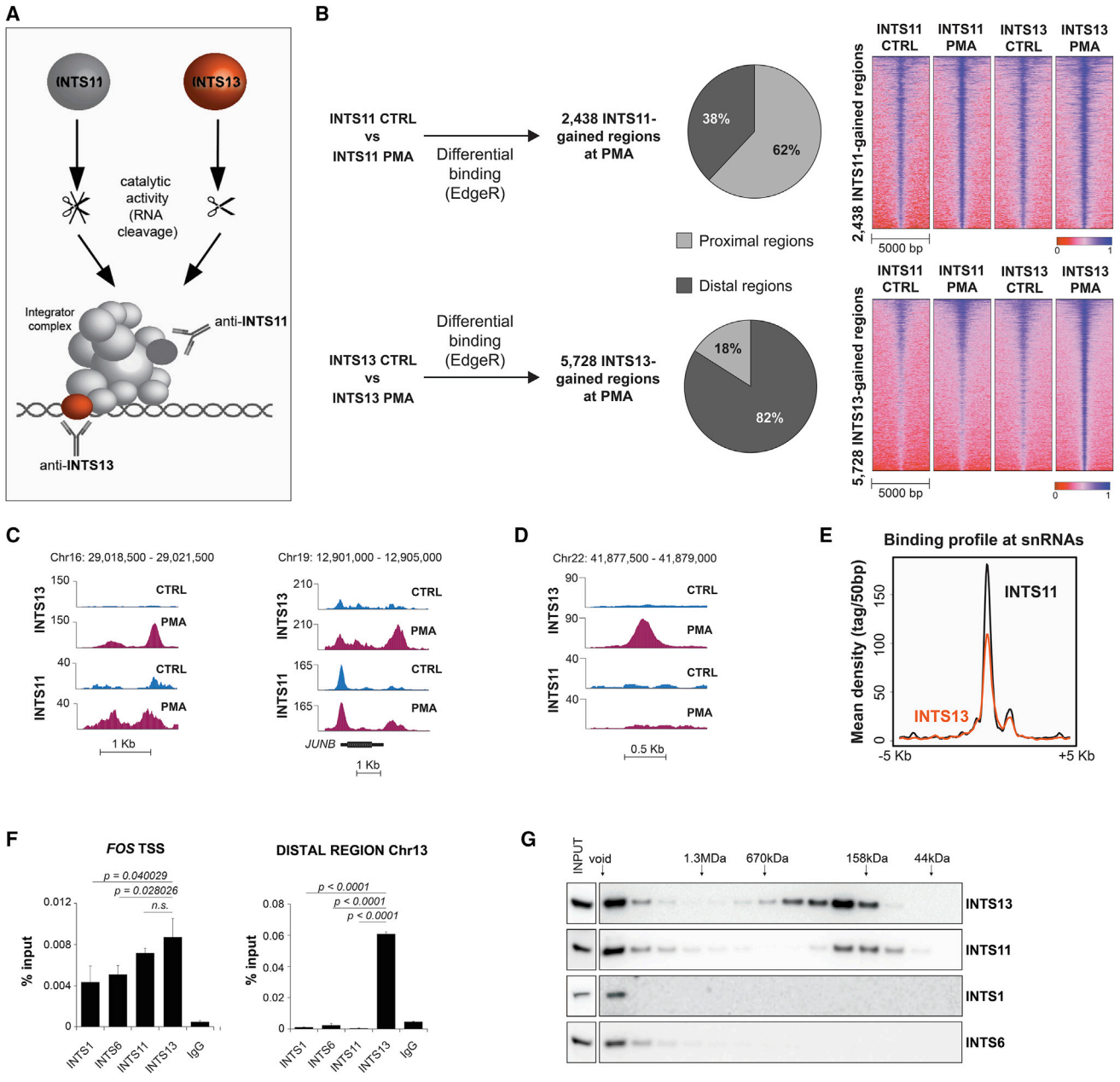

Figure 3. Modular Properties of the Integrator Complex during Myeloid Differentiation

(A) Schematic panel describing the experimental pipeline. The catalytic activity of Integrator is impaired by INTS11 depletion, while it is not affected upon INTS13 depletion. The chromatin occupancy of the two subunits was profiled in undifferentiated (CTRL) and differentiated (PMA) cells by ChIP-seq with specific polyclonal antibodies.

(B) Schematic panel describing the analytical pipeline. A differential binding analysis between CTRL and PMA conditions for INTS11 and INTS13 (edgeR, FDR <10%) detected 2,438 INTS11-gained and 5,728 INTS13-gained regions, respectively. The majority of the INTS11-gained regions are proximal to protein coding genes (distance <1 kb from nearest TSS), while the large majority of INTS13-gained regions are distal (distance >1 kb from TSS). INTS13 is bound to all of the INTS11-gained regions. Conversely, a fraction of INTS13-gained regions is devoid of INTS11.

(C) An intronic region within the *CD84* gene on Chr16 and the *JUNB* locus both display robust recruitment of INTS11 and INTS13 upon PMA induction.

(D) An intergenic region on Chr22 shows significant recruitment of INTS13, but not INTS11.

(E) Average profile of INTS11 and INTS13 at all active U snRNAs (Gencode annotation) displays stronger enrichment of INTS11 compared to INTS13, suggesting that the INTS11 antibody performs well in ChIP-seq.

(F) ChIP-qPCR on the TSS of *FOS* shows comparable enrichment for multiple INTS subunits, while the qPCR performed on a distal INTS13-gained regions suggests that INTS13 is the sole INTS subunit recruited. Data are means ± SD.

(legend continued on next page)

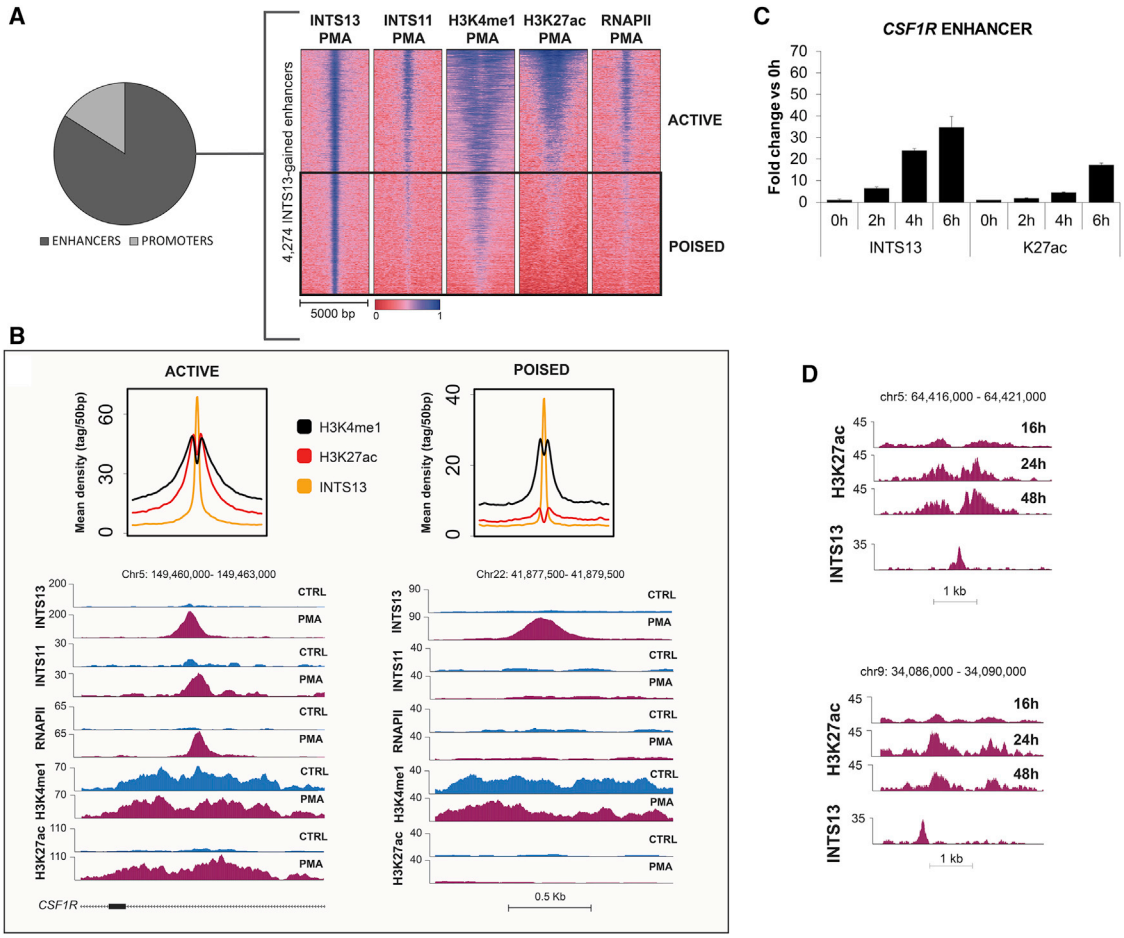

Figure 4. INTS13 at Active and Poised Enhancers during Monocytic Differentiation

(A) 4,274 of the 5,728 INTS13-gained regions are distal elements. The heatmap shows (K-means clustering) that nearly half of these distal elements are active enhancers (enriched for INTS13, INTS11, RNAPII, and the chromatin marks H3K27ac, H3K4me1), while the other half likely represent poised/inactive enhancers, enriched for INTS13 and the chromatin mark H3K4me1.

(B) Average profiles of H3K27ac, H3K4me1 and INTS13 at active and poised enhancers, with representative examples.

(C) ChIP-qPCR of INTS13 and H3K27ac during a time course of early PMA induction (0, 2, 4, and 6 hr) for the *CSF1R* enhancer supports a model in which INTS13 binding precedes the activation of the enhancer. Data are means ± SD.

(D) Screenshots for two INTS13-gained enhancers classified as poised at 16 hr of PMA induction. These enhancers show increase of H3K27ac levels suggesting their activation at a later time point following INTS13 binding.

observed co-localization of EGR1 and INTS13 genome-wide (Figures 5B and 5C). Motif analysis of EGR1 also retrieved an EGR1/2 matrix nearly identical to that of INTS13 (Figure S5G). ChIP-qPCR assay confirmed that EGR1 and EGR2 as both present at select monocytic enhancers, suggesting their functional redundancy in our system (Figure S5H). We reasoned that binding of EGR1/2 may be a prerequisite for INTS13 binding to enhancers. To assess the importance of EGR1/2 in recruiting Integrator, we performed ChIP-seq of INTS13 after depletion of EGR1 in HL-60 (Figures 5D, 5E, and S5). INTS13 recruitment at enhancers was significantly impaired by EGR1 knockdown (Wilcoxon's rank-sum test, $p < 2.2 \times 10^{-16}$, Figures 5D and 5E). While some INTS13 binding persisted, it must be noted that *EGR2* is still expressed in these cells, even if a much lower level compared to *EGR1*, and that double depletion bears acute effects on survival and cell cycle (Laslo et al., 2006). Furthermore, we tested the overlap of INTS13 and EGR1 peaks pre- and post-stimulation of PMA. In undifferentiated cells, EGR1 colocalized with ~5% of INTS13 sites. Conversely, monocytic differentiation boosted the share of overlapping peaks to ~40% (Figure 5F).

(G) Nuclear extract of HL-60 cells was fractionated on a Superose 6 chromatography column in the presence of 0.5 M KCl. All Integrator subunits eluted with the high-molecular-weight fractions, corresponding to the intact complex. Additionally, INTS11 elutes in a known lower-molecular-weight interaction with the other catalytic subunit, INTS9. INTS13 is detected eluting with lower-molecular-weight fractions that differ from INTS11 and other Integrator subunits, suggesting that INTS13 can associate separately from the full complex in the nucleoplasm. Molecular weight standards are labeled above. Lanes are as follows: input, even fractions 20–46.

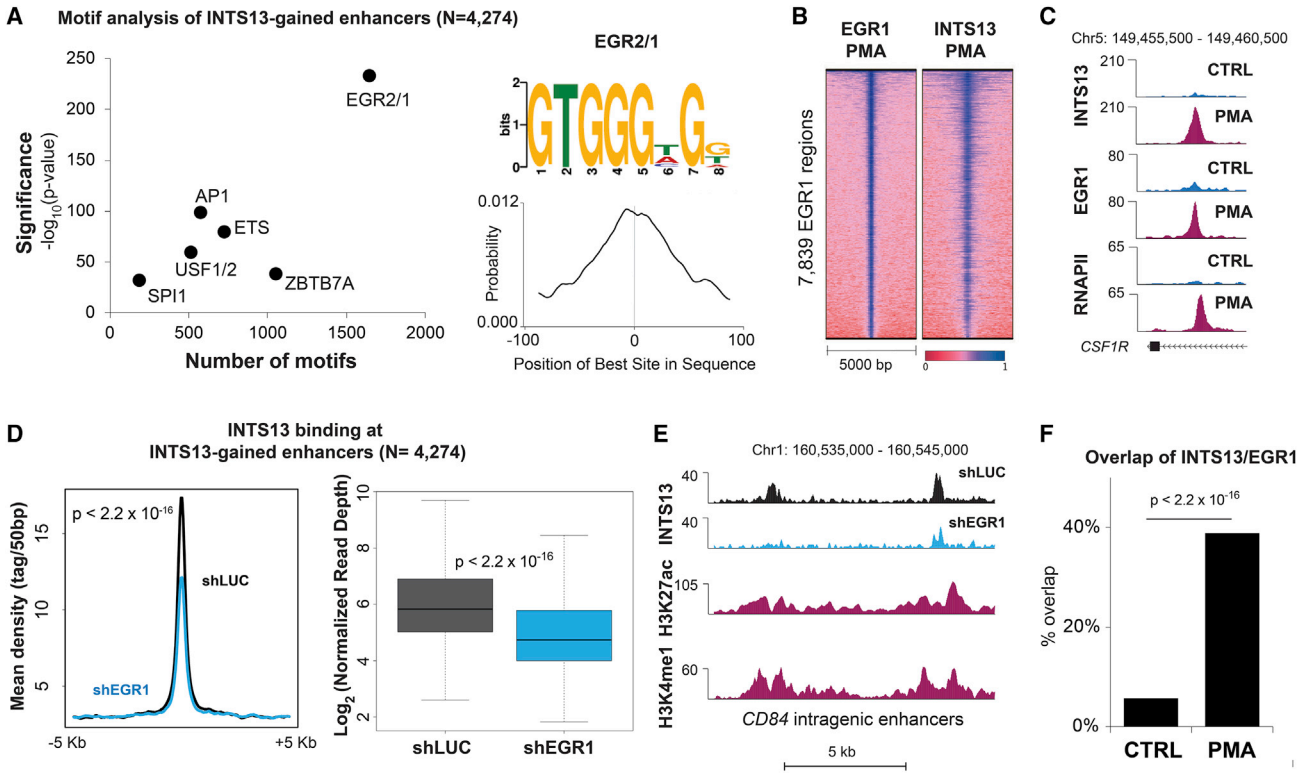

Figure 5. INTS13 Targets EGR Responsive Sites Genome-wide

(A) *De novo* motif analysis of 4,274 INTS13-gained enhancers (summits ±100 bp). The EGR2/1 motif is the most significantly and centrally enriched. p value of significance are plotted on the y axis, motif recurrence (total number of sites) is plotted on the x axis.

(B) EGR1 sites overlap INTS13 sites genome-wide, in differentiating HL-60 cells. The heatmap represents intensity of EGR1 and INTS13 ChIP-seq binding across all EGR1 peaks (PMA-stimulated cells).

(C) Screenshot of the *CSF1R* intronic enhancer shows a significant recruitment of INTS13 and EGR1.

(D) Depletion of EGR1 significantly reduces the binding of INTS13 at all of the 4,274 INTS13-gained enhancers in PMA-stimulated HL-60 cells (Wilcoxon rank-sum test $p < 2.2 \times 10^{-16}$).

(E) Two intragenic enhancers of the *CD84* locus are shown to exemplify loss of INTS13 upon EGR1 depletion.

(F) The overlap between INTS13 and EGR1 peaks significantly increases (5%–40%) upon PMA induction in HL-60 cells (Wilcoxon rank-sum test $p < 2.2 \times 10^{-16}$).

Collectively, we demonstrated that EGR1 is a determinant of INTS13 binding at enhancers during monocytic differentiation, while progenitor cells maintain distinct binding profiles for both. These data suggest that additional factors may be required to draw INTS13 to EGR1-responsive elements.

NAB2 Is an Essential Co-factor for Enhancer Activation Mediated by INTS13 and EGR1/2

We surmised that INTS13 binding to EGR1/2 at enhancers may be overall mediated by protein-protein interactions; therefore, we performed proteomic analysis of untreated and differentiating HL-60 cells in two independent replicates. We used rabbit antibodies to immunoprecipitate endogenous INTS13 and subjected the eluate to liquid chromatography-tandem mass spectrometry (LC-MS/MS) analysis. As expected, INTS13 co-precipitated the full Integrator complex and subunits of RNAPII (Figure 6A; Table S2). Next, we looked for non-Integrator components in our proteomic analysis. We previously described that widespread recruitment of INTS13 to EGR1/2 monocytic enhancers (Figures 3 and 5) is specific to differentiating monocytes. In fact, INTS13 is largely dispensable for undifferentiated progenitor cells but is required for maturation into functional monocytes/macrophages (Figures 2 and S2). We reasoned that additional protein partners of INTS13 may be specific to differentiating cells; therefore, we calculated the ratio of peptides retrieved in differentiating (PMA) over undifferentiated (CTRL) HL-60 cells. Notably, we identified the NGFI-A-binding protein 2 (NAB2) as the most significantly enriched protein. NGFI-A is an alias for EGR1, since NAB2 and its functional homolog, NAB1, were originally identified as partners of EGR1 and EGR2 (Russo et al., 1995, Svaren et al., 1996). We confirmed the association of NAB2 with INTS13 by co-immunoprecipitation experiments from the nuclear extract of HL-60 cells and observed that NAB2 was lowly abundant in untreated cells but accumulated upon differentiation (Figure 6B). Importantly, we observed a similar regulation in primary cells: NAB2 was barely detectable in primary human stem and progenitor cells ($CD34^+$) and increased dramatically during monocytic differentiation stimulated by M-CSF (Figure S6). To further validate the interaction of NAB2 with INTS13/Integrator, we

generated stable cell clones expressing FLAG-tagged NAB2 and performed a reverse LC-MS/MS experiment. FLAG affinity purification of NAB2 complexes co-purified the EGR proteins and INTS13, along with several other subunits of Integrator (Figure 6C). Our data imply that NAB2 bridges the interaction of INTS13 with EGR1/EGR2 and suggest that a ternary complex composed of INTS13/NAB2/EGR may form at monocytic enhancers. We performed ChIP-seq of endogenous NAB2 in HL-60 cells and found a distinct distribution of NAB2 peaks during differentiation. Consistent with INTS13, NAB2 showed a significant recruitment at the 4,274 monocytic enhancers (Figure 6D), colocalizing with EGR1 and INTS13 at most of these sites (Figures 6D, 6E, and S6). Interestingly, best correlation between INTS13 and EGR1 happens on NAB2 peaks (Figure S6C). Notably, NAB2 binding dynamics resembled those of INTS13, preceding acetylation of the enhancer, such as in *CSF1R* (Figure S6). Further, ChIP-seq on PMA-induced HL-60 showed that INTS13 binding at the 4,274 monocytic enhancers was severely impaired by NAB2 depletion (two independent shRNAs; $p < 0.0001$; Figures 6F, 6G, and S6). This suggested NAB2 as the molecular bridge that recruits INTS13 to EGR1/2-responsive elements. Moreover, 679 genes were DE in PMA-treated HL-60 upon NAB2-KD (517 downregulated, FDR <5%, Figures 6H and 6I). IPA analysis confirmed enrichment in hematopoiesis pathways (Figures 6H, 6I, and S6), thus recapitulating the results obtained upon depletion of INTS13 (Figures 2B–2D).

If NAB2 is an essential co-factor that elicits enhancer activation via recruitment of INTS13, depletion of NAB2 should also impair development of monocytic/macrophagic cells and phenocopy the effect of either INTS13 depletion (Figures 1F and 1H) or EGR1 depletion (Laslo et al., 2006). Coherently, both NAB2 and EGR1 were indeed required for differentiation of HL-60 cells (mean fluorescence intensity [MFI] of CD11b, Figure 6J) and were essential to form M-CSF-derived monocytic colonies from $CD34^+$ stem and progenitor cells (Figures 6K and S6).

To further validate the INTS13/NAB2 functional association in physiological conditions, we performed additional ChIP-seq experiments using circulating monocytes obtained from the peripheral blood of healthy donors. Terminal differentiation of monocytes into adherent macrophages reignites the enhancer-promoter network that is responsible for the earlier differentiation stages ($CD34^+$ to monocytes) and provides a physiological model for enhancer regulation (Heinz et al., 2010; Pham et al., 2012). Consistent with our findings from HL-60, the ChIP-seq data from the differentiating macrophages supported a significant recruitment of both INTS13 and NAB2 at the previously identified 4,274 monocytic enhancers, including *CSF1R* (Figure S7). Furthermore, we independently depleted EGR1 and NAB2 from a pool of mobilized $CD34^+$ cells, performed INTS13 ChIP-seq at day 5 of monocytic differentiation, and observed, in both cases, a sharp and significant decrease of INTS13 across all the genome (Figure S7). Together, the data obtained in primary cells fully support our previous findings in HL-60 cells, and in particular the role of NAB2 and EGR1 in the recruitment of INTS13 at thousands of lineage-specific enhancers.

The INTS13/EGR/NAB2 Axis Brings about Activation of Poised Enhancers

We performed chromosome conformation capture (3C) on the enhancer of *CSF1R* to infer the consequences of INTS13 depletion on genome architecture. During differentiation of HL-60 cells, we detected a robust interaction between the intronic enhancer of *CSF1R* and the proximal promoter, as compared to other regions within the *CSF1R* gene or with the promoter of neighboring genes (Figure 7A). Specifically, we observed an ~5-fold decrease in the frequency of enhancer-promoter interactions following depletion of INTS13, while all non-specific contact pairs used as controls (NEG1 to NEG5) were not affected (Figure 7A). This assay demonstrated the functional requirement of INTS13 for enhancer-promoter looping of a monocytic enhancer engaged during differentiation.

Collectively, our data demonstrated that INTS13/Integrator targets poised enhancers that are required for monocytic differentiation. While these enhancers are primarily bound by the EGR1/2 TFs, the co-factor NAB2 is the essential molecular bridge that allows binding of INTS13 to EGR-dependent enhancers. Altogether, the INTS13/EGR1/NAB2 axis is functionally required to coordinate and elicit activation of monocytic and macrophagic genes during myeloid differentiation (Figure 7B).

DISCUSSION

In this work, we characterize a novel function of the Integrator protein complex and demonstrate that an accessory (non-catalytic) subunit of a general activator machinery can operate as a mediator of lineage-determining TFs. We characterize a novel mechanism of enhancer regulation, in which a co-activator subunit (INTS13), a DNA-binding TF (EGR1/2), and a non-DNA-binding co-factor (NAB2) take part. We demonstrate co-occupancy of this ternary complex at chromatin and capture their physical interaction by co-immunoprecipitation and LC-MS/MS. Our data suggest that the INTS13/EGR/NAB2 axis is a priming complex for enhancers. In fact, we initially found that INTS13/EGR/NAB2 bind to active and poised enhancers. Poised enhancers, which lack H3K27 acetylation but retain mono-methylation of H3K4, have been previously described in differentiated and multipotent cells (Creyghton et al., 2010; Ostuni et al., 2013; Rada-Iglesias et al., 2011; Zentner et al., 2011). We showed that INTS13 and NAB2 target poised enhancers during monocytic differentiation, preceding the wave of H3K27 hyperacetylation. Persistently poised enhancers, which we detect after 16 hr of PMA stimulation, may become activated at a later time point, as our data suggest. It is also possible that additional co-factors are needed to elicit activation of a subset of INTS13/EGR1/NAB2 targets. Importantly, enhancers regulated by INTS13, EGR1, and NAB2 are required for proper expression of genes that confer monocytic identity. Our analysis of EGR1 represents the first profiling of this zinc finger TF in differentiating progenitors and reveals the unexpected breadth of its role as a lineage-determining factor via enhancer regulation. TFs such as PU.1 and ERG (Ets) are generally considered master regulators of myeloid commitment (Álvarez-Errico et al., 2015). In fact, when we searched for DNA motifs associated with INTS13-enhancers, we retrieved both PU.1 and ERG, though less significantly enriched than

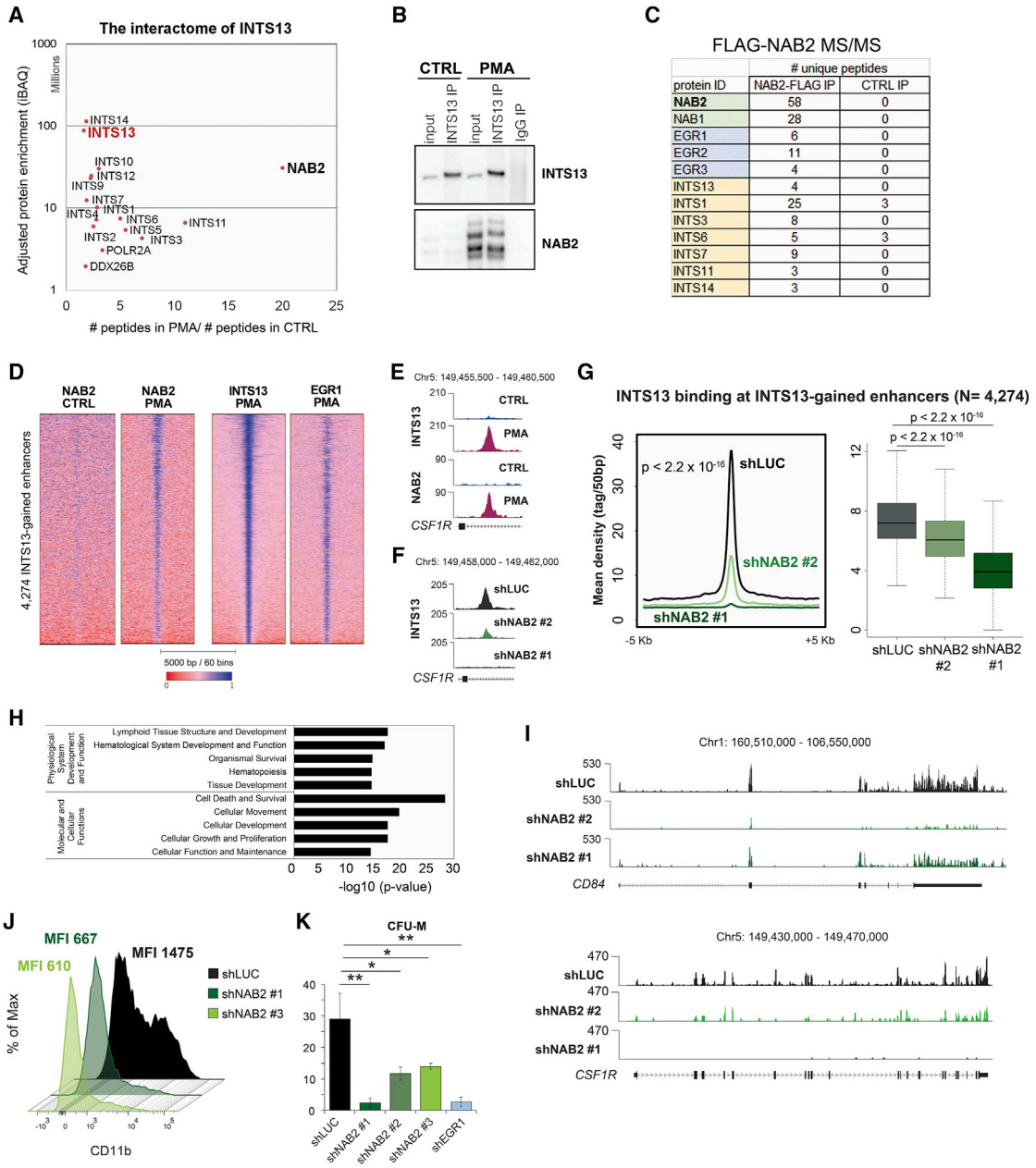

Figure 6. NAB2 Is an Essential Co-factor of Monocytic Differentiation and Mediates INTS13 Binding at EGR1 Sites

(A) Endogenous INTS13 was affinity-purified from undifferentiated and differentiating HL-60 cells. The interactome of INTS13 was detected by LC-MS/MS. The plot shows adjusted protein enrichment values (iBAQ, y axis) and the ratio of peptides in differentiated (PMA) versus undifferentiated (CTRL) cells. INTS13 interacts with nearly all Integrator subunits and RNAPII, interaction with the EGR1 co-factor NAB2 is specific to monocytic differentiation.

(B) Immunoprecipitation of INTS13 in undifferentiated (CTRL) and differentiated (PMA) HL-60 cells confirms the interaction between INTS13 and NAB2 after PMA treatment.

(C) LC-MS/MS analysis of stable HL-60 clones expressing exogenous FLAG-NAB2. NAB2 was affinity purified by anti-FLAG conjugated beads. NAB2 interacts with NAB1, EGR-family members (EGR1, EGR2, EGR3), INTS13, and other Integrator subunits.

(D) Heatmaps of NAB2, INTS13, and EGR1 ChIP-seq in undifferentiated (CTRL) and/or differentiated (PMA) HL-60. Upon PMA treatment, NAB2, INTS13, and EGR1 co-localize at INTS13-gained enhancers.

(E) Screenshot of the intragenic *CSF1R* enhancer shows recruitment of NAB2 and INTS13 during differentiation.

(F) Screenshot of the *CSF1R* intragenic enhancer shows reduction of INTS13 recruitment upon NAB2 depletion.

(G) Average profiles and box-plot display a significant decrease of INTS13 at the 4,274 INTS13-gained enhancers upon NAB2-KD (two different shRNAs).

(H) RNA-seq analysis identified 517 genes downregulated upon NAB2-KD (two different shRNAs) during PMA-induced differentiation. IPA analysis for these genes revealed enrichment for pathways associated to hematopoiesis and differentiation, recapitulating the results previously obtained with INTS13 depletion (Figure 2).

(legend continued on next page)

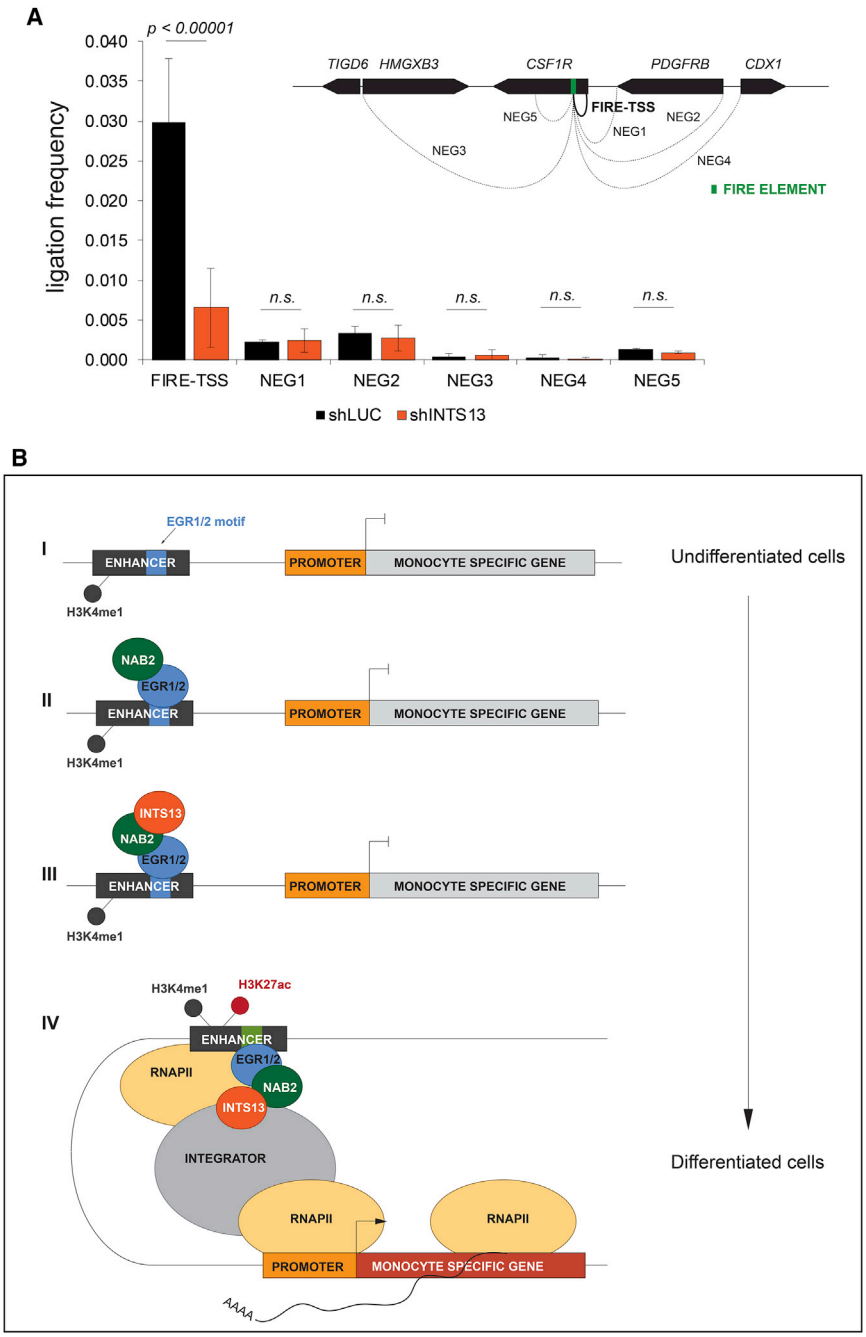

Figure 7. Targeted Enhancer Activation by INTS13

(A) Chromosome conformation capture (3C) reveals that depletion of INTS13 elicits a significant reduction of the interaction frequency between the intragenic enhancer of *CSF1R* (FIRE element) and the promoter of the same gene, suggesting that INTS13 mediates loop formation, enhancer/promoter interaction, and ultimately the expression of the *CSF1R* (see also Figure 2D). As control, we gauged the interaction frequency between the enhancer (anchor) and 5 additional surrounding sites (NEG1 to NEG5), including the TSS of 3 additional genes, the 3′ end of one gene and a non-enhancer intronic region of *CSF1R*. Data are means ± SD.

(B) We propose a model for the role of Integrator in targeted enhancer activation during cell differentiation. In undifferentiated cells, lineage-specific genes are not expressed, and their corresponding enhancers are inactive or poised (I). Upon lineage commitment, EGR1 recognizes and binds to its motifs across monocytic enhancers, together with NAB2 (II). INTS13 is recruited by the NAB2/EGR1 complex, and co-localizes at the same enhancers (III). Following INTS13 priming of the enhancers, the Integrator complex is assembled, facilitating enhancer activation and chromatin looping to ultimately activate transcription of the target genes (IV).

EGR1 and not centrally positioned with respect to the INTS13 peak summit, underscoring that the Integrator complex preferentially operates via EGR1 during monocytic differentiation. EGR1 and EGR2 were previously proposed to regulate monocytic differentiation by repressing granulocytic genes (Krishnaraju et al., 2001; Laslo et al., 2006; Nguyen et al., 1993). Instead, our data suggest that EGR1 and EGR2 (which we find functionally redundant by ChIP and proteomic analyses) directly regulate enhancer-mediated activation of monocytic- and macrophagic-specific genes, such as *CSF1R*. Furthermore, we revealed an essential and unexpected role of the co-factor NAB2. EGR1 and EGR2 were previously shown to interact with NAB2 by two-hybrid and *in vitro* pull-down experiments; such interaction is deemed important for neuronal differentiation and development (Kumbrink et al., 2005, 2010; Svaren et al., 1996). Previous biochemical evidences suggested that NAB2 merely served as co-repressor for a subset of EGR1 target promoters (Lucerna et al., 2003; Svaren et al., 1996). Our data reveal, instead, that NAB2 functions as a molecular switch, determining INTS13 recruitment at EGR1 sites in both primary and HL-60 cells. Furthermore, depletion of NAB2 phenocopies loss of INTS13 and EGR1: cell lines and primary

(I) Prototypical monocytic genes such as *CSF1R* and *CD84* are severely downregulated by NAB2 depletion in RNA-seq experiments.

(J) Mean fluorescence intensity of CD11b is impaired in differentiated HL-60 cells after depletion of NAB2 with two different shRNAs (16 hr post-PMA induction).

(K) Colony-forming unit (CFU) assay of cord-blood-derived $CD34^+$ cells infected with shRNAs against NAB2 and EGR1 shows that the number of monocytic/macrophagic colonies is significantly reduced in both NAB2- and EGR1-depleted cells when compared to control. Data are means ± SD.

$CD34^+$ cells depleted of NAB2 fail to activate a monocytic transcriptome and are blocked at a progenitor stage. Collectively, we present the first comprehensive molecular characterization of NAB2 and provide the first evidence of NAB2 binding profile at chromatin. We propose that the role of NAB2 in myeloid differentiation is to regulate timely activation of monocytic enhancers by recruiting INTS13. Beyond monocytic differentiation, EGR1/NAB2-dependent enhancers may play a role in other developmental pathways. For instance, we suggest that T cell activation may also require INTS13 as a modulator of EGR1 sites. Also, EGR1 and NAB2 were previously implicated in neural development, raising the possibility that INTS13 is a major effector of cell commitment and differentiation in such context.

Another critical finding of our work is that the Integrator complex is not functionally homogeneous. In particular, we focus on the INTS13 subunit, which was recently described as an integral component of the human and *Drosophila* Integrator complexes (Chen et al., 2012; Malovannaya et al., 2011). Our data show that INTS13 is, *de facto*, a physical and functional submodule of Integrator. INTS13 is part of the full Integrator complex in myeloid cells (Figures 1A, 3G, and 6A) but can also exist as a small subcomplex (perhaps associated with additional INTS subunits, Figure 3G). INTS13 is not required for the core catalytic activity of Integrator (RNA endonucleolysis), nor is it essential for cell growth of progenitor and stem cells under resting conditions (Figure 1) but is indispensable for cell commitment and differentiation. Unlike INTS11, INTS9, and INTS1 (Baillat et al., 2005; Chen et al., 2012), INTS13 is dispensable for processing of U snRNAs and, likely, for termination of noncoding eRNAs that employs the same catalytic activity centered around the β-CASP domain of INTS11 (Lai et al., 2015). A previous report suggested that INTS13 (also known as ASUN) had an influence on U snRNA processing (Chen et al., 2012). However, the effect of INTS13 depletion on a GFP-UsnRNA reporter system was significantly lower than the effect of INTS9 depletion (Chen et al., 2012). Furthermore, reporter constructs may not entirely reflect Integrator's activity at endogenous U snRNA loci. However, we cannot exclude that INTS13 may retain regulatory activity toward U snRNA processing in lower eukaryotes. Further studies are needed to address the evolution of the Integrator complex and to determine the complete map of *core* and *accessory* subunits of this essential transcriptional regulator.

In conclusion, our data suggest that large and ubiquitously expressed co-activator complexes are not just passive facilitators of transcription but may actively partake in the organization of cell- and tissue-specific enhancer-promoter activity.

STAR★METHODS

Detailed methods are provided in the online version of this paper and include the following:

- KEY RESOURCES TABLE
- CONTACT FOR REAGENT AND RESOURCE SHARING
- EXPERIMENTAL MODEL AND SUBJECT DETAILS
  - Cell lines
  - Primary cells
- METHOD DETAILS
  - Lentiviral infection
  - *In vitro* differentiation
  - Knockdown of INTS11, INTS13, EGR1 and NAB2
  - NAB2 overexpression
  - Western blot
  - Real-time quantitative polymerase chain reaction
  - Colony-forming unit (CFU) assays
  - Proliferation assay
  - Immunoprecipitation
  - Size-exclusion chromatography
  - Antibody crosslinking
  - Mass spectrometry
  - Chromosome conformation capture (3C)
  - ChIP-seq and ChIP-qPCR sample processing
  - ChIP-seq analyses
  - Subcellular fractionation
  - RNA-seq sample processing
  - RNA-seq analyses
- QUANTIFICATION AND STATISTICAL ANALYSIS
- DATA AND SOFTWARE AVAILABILITY

SUPPLEMENTAL INFORMATION

Supplemental Information includes seven figures, four tables, and three data files and can be found with this article online at https://doi.org/10.1016/j.molcel.2018.05.031.

ACKNOWLEDGMENTS

This work was supported by a Leukemia Research Foundation award to A.G. S.A.W. is supported by NIH training grant T32-GM071339. We thank Paul Lieberman and Rugang Zhang for helpful discussions and Alessandra De Leo for technical help with 3C. We are grateful to the Wistar Core Facilities for generating and processing the data presented: Genomics Core, Dr. Shashi Bala; Proteomics Core, Hsin-Yao Tang and Thomas Beer; Flow Cytometry Core, Jeffrey Faust (NCI CCSG: P30-CA010815).

AUTHOR CONTRIBUTIONS

E.B., M.T., and A.G. designed the experiments. E.B., M.T., S.A.W., and T.A.O. performed the experiments. M.T. performed all computational and statistical analyses. B.C. and M.C. provided primary samples and technical support for their manipulation. K.S. provided technical support for the chromatography experiments and critical review of the manuscript. E.B., M.T., and A.G. wrote the paper. All co-authors read and approved the manuscript.

DECLARATION OF INTERESTS

The authors declare no competing interests.

Received: November 8, 2017
Revised: April 11, 2018
Accepted: May 24, 2018
Published: June 28, 2018

REFERENCES

Albrecht, T.R., and Wagner, E.J. (2012). snRNA 3′ end formation requires heterodimeric association of integrator subunits. Mol. Cell. Biol. *32*, 1112–1123.

Álvarez-Errico, D., Vento-Tormo, R., Sieweke, M., and Ballestar, E. (2015). Epigenetic control of myeloid cell differentiation, identity and function. Nat. Rev. Immunol. *15*, 7–17.

Baillat, D., Hakimi, M.A., Näär, A.M., Shilatifard, A., Cooch, N., and Shiekhattar, R. (2005). Integrator, a multiprotein mediator of small nuclear RNA processing, associates with the C-terminal repeat of RNA polymerase II. Cell *123*, 265–276.

Barozzi, I., Simonatto, M., Bonifacio, S., Yang, L., Rohs, R., Ghisletti, S., and Natoli, G. (2014). Coregulation of transcription factor binding and nucleosome occupancy through DNA features of mammalian enhancers. Mol. Cell *54*, 844–857.

Bender, A.T., and Beavo, J.A. (2006). PDE1B2 regulates cGMP and a subset of the phenotypic characteristics acquired upon macrophage differentiation from a monocyte. Proc. Natl. Acad. Sci. USA *103*, 460–465.

Bose, D.A., Donahue, G., Reinberg, D., Shiekhattar, R., Bonasio, R., and Berger, S.L. (2017). RNA binding to CBP stimulates histone acetylation and transcription. Cell *168*, 135–149.

Chen, J., Ezzeddine, N., Waltenspiel, B., Albrecht, T.R., Warren, W.D., Marzluff, W.F., and Wagner, E.J. (2012). An RNAi screen identifies additional members of the Drosophila Integrator complex and a requirement for cyclin C/Cdk8 in snRNA 3′-end formation. RNA *18*, 2148–2156.

Cox, J., and Mann, M. (2008). MaxQuant enables high peptide identification rates, individualized p.p.b.-range mass accuracies and proteome-wide protein quantification. Nat. Biotechnol. *26*, 1367–1372.

Creyghton, M.P., Cheng, A.W., Welstead, G.G., Kooistra, T., Carey, B.W., Steine, E.J., Hanna, J., Lodato, M.A., Frampton, G.M., Sharp, P.A., et al. (2010). Histone H3K27ac separates active from poised enhancers and predicts developmental state. Proc. Natl. Acad. Sci. USA *107*, 21931–21936.

Dekker, J., Rippe, K., Dekker, M., and Kleckner, N. (2002). Capturing chromosome conformation. Science *295*, 1306–1311.

Dobin, A., Davis, C.A., Schlesinger, F., Drenkow, J., Zaleski, C., Jha, S., Batut, P., Chaisson, M., and Gingeras, T.R. (2013). STAR: Ultrafast universal RNA-seq aligner. Bioinformatics *29*, 15–21.

Egloff, S., Szczepaniak, S.A., Dienstbier, M., Taylor, A., Knight, S., and Murphy, S. (2010). The integrator complex recognizes a new double mark on the RNA polymerase II carboxyl-terminal domain. J. Biol. Chem. *285*, 20564–20569.

Friedman, A.D. (2007). Transcriptional control of granulocyte and monocyte development. Oncogene *26*, 6816–6828.

Gallagher, R., Collins, S., Trujillo, J., McCredie, K., Ahearn, M., Tsai, S., Metzgar, R., Aulakh, G., Ting, R., Ruscetti, F., and Gallo, R. (1979). Characterization of the continuous, differentiating myeloid cell line (HL-60) from a patient with acute promyelocytic leukemia. Blood *54*, 713–733.

Gardini, A., Baillat, D., Cesaroni, M., Hu, D., Marinis, J.M., Wagner, E.J., Lazar, M.A., Shilatifard, A., and Shiekhattar, R. (2014). Integrator regulates transcriptional initiation and pause release following activation. Mol. Cell *56*, 128–139.

Giudicelli, F., Taillebourg, E., Charnay, P., and Gilardi-Hebenstreit, P. (2001). Krox-20 patterns the hindbrain through both cell-autonomous and non cell-autonomous mechanisms. Genes Dev. *15*, 567–580.

Heinz, S., Benner, C., Spann, N., Bertolino, E., Lin, Y.C., Laslo, P., Cheng, J.X., Murre, C., Singh, H., and Glass, C.K. (2010). Simple combinations of lineage-determining transcription factors prime cis-regulatory elements required for macrophage and B cell identities. Mol. Cell *38*, 576–589.

Heinz, S., Romanoski, C.E., Benner, C., and Glass, C.K. (2015). The selection and function of cell type-specific enhancers. Nat. Rev. Mol. Cell Biol. *16*, 144–154.

Himes, S.R., Tagoh, H., Goonetilleke, N., Sasmono, T., Oceandy, D., Clark, R., Bonifer, C., and Hume, D.A. (2001). A highly conserved c-fms gene intronic element controls macrophage-specific and regulated expression. J. Leukoc. Biol. *70*, 812–820.

Hsieh, C.L., Fei, T., Chen, Y., Li, T., Gao, Y., Wang, X., Sun, T., Sweeney, C.J., Lee, G.S., Chen, S., et al. (2014). Enhancer RNAs participate in androgen receptor-driven looping that selectively enhances gene activation. Proc. Natl. Acad. Sci. USA *111*, 7319–7324.

Huang, J., Liu, X., Li, D., Shao, Z., Cao, H., Zhang, Y., Trompouki, E., Bowman, T.V., Zon, L.I., Yuan, G.C., et al. (2016). Dynamic control of enhancer repertoires drives lineage and stage-specific transcription during hematopoiesis. Dev. Cell *36*, 9–23.

Krishnaraju, K., Hoffman, B., and Liebermann, D.A. (2001). Early growth response gene 1 stimulates development of hematopoietic progenitor cells along the macrophage lineage at the expense of the granulocyte and erythroid lineages. Blood *97*, 1298–1305.

Krysinska, H., Hoogenkamp, M., Ingram, R., Wilson, N., Tagoh, H., Laslo, P., Singh, H., and Bonifer, C. (2007). A two-step, PU.1-dependent mechanism for developmentally regulated chromatin remodeling and transcription of the c-fms gene. Mol. Cell. Biol. *27*, 878–887.

Kumbrink, J., Gerlinger, M., and Johnson, J.P. (2005). Egr-1 induces the expression of its corepressor nab2 by activation of the nab2 promoter thereby establishing a negative feedback loop. J. Biol. Chem. *280*, 42785–42793.

Kumbrink, J., Kirsch, K.H., and Johnson, J.P. (2010). EGR1, EGR2, and EGR3 activate the expression of their coregulator NAB2 establishing a negative feedback loop in cells of neuroectodermal and epithelial origin. J. Cell. Biochem. *111*, 207–217.

Lai, F., Gardini, A., Zhang, A., and Shiekhattar, R. (2015). Integrator mediates the biogenesis of enhancer RNAs. Nature *525*, 399–403.

Laslo, P., Spooner, C.J., Warmflash, A., Lancki, D.W., Lee, H.J., Sciammas, R., Gantner, B.N., Dinner, A.R., and Singh, H. (2006). Multilineage transcriptional priming and determination of alternate hematopoietic cell fates. Cell *126*, 755–766.

Li, H. (2013). Aligning sequence reads, clone sequences and assembly contigs with BWA-MEM. arXiv:, arXiv:1303.3997, https://arxiv.org/abs/1303.3997.

Li, B., and Dewey, C.N. (2011). RSEM: Accurate transcript quantification from RNA-seq data with or without a reference genome. BMC Bioinformatics *12*, 323.

Li, H., Handsaker, B., Wysoker, A., Fennell, T., Ruan, J., Homer, N., Marth, G., Abecasis, G., and Durbin, R.; 1000 Genome Project Data Processing Subgroup (2009). The Sequence Alignment/Map format and SAMtools. Bioinformatics *25*, 2078–2079.

Li, W., Notani, D., Ma, Q., Tanasa, B., Nunez, E., Chen, A.Y., Merkurjev, D., Zhang, J., Ohgi, K., Song, X., et al. (2013). Functional roles of enhancer RNAs for oestrogen-dependent transcriptional activation. Nature *498*, 516–520.

Liao, Y., Smyth, G.K., and Shi, W. (2014). featureCounts: An efficient general purpose program for assigning sequence reads to genomic features. Bioinformatics *30*, 923–930.

Love, M.I., Huber, W., and Anders, S. (2014). Moderated estimation of fold change and dispersion for RNA-seq data with DESeq2. Genome Biol. *15*, 550.

Lucerna, M., Mechtcheriakova, D., Kadl, A., Schabbauer, G., Schäfer, R., Gruber, F., Koshelnick, Y., Müller, H.D., Issbrücker, K., Clauss, M., et al. (2003). NAB2, a corepressor of EGR-1, inhibits vascular endothelial growth factor-mediated gene induction and angiogenic responses of endothelial cells. J. Biol. Chem. *278*, 11433–11440.

Malovannaya, A., Lanz, R.B., Jung, S.Y., Bulynko, Y., Le, N.T., Chan, D.W., Ding, C., Shi, Y., Yucer, N., Krenciute, G., et al. (2011). Analysis of the human endogenous coregulator complexome. Cell *145*, 787–799.

Nguyen, H.Q., Hoffman-Liebermann, B., and Liebermann, D.A. (1993). The zinc finger transcription factor Egr-1 is essential for and restricts differentiation along the macrophage lineage. Cell *72*, 197–209.

Ostuni, R., Piccolo, V., Barozzi, I., Polletti, S., Termanini, A., Bonifacio, S., Curina, A., Prosperini, E., Ghisletti, S., and Natoli, G. (2013). Latent enhancers activated by stimulation in differentiated cells. Cell *152*, 157–171.

Pham, T.H., Benner, C., Lichtinger, M., Schwarzfischer, L., Hu, Y., Andreesen, R., Chen, W., and Rehli, M. (2012). Dynamic epigenetic enhancer signatures reveal key transcription factors associated with monocytic differentiation states. Blood *119*, e161–e171.

Poirier, R., Cheval, H., Mailhes, C., Garel, S., Charnay, P., Davis, S., and Laroche, S. (2008). Distinct functions of egr gene family members in cognitive processes. Front. Neurosci. *2*, 47–55.

Quinlan, A.R., and Hall, I.M. (2010). BEDTools: A flexible suite of utilities for comparing genomic features. Bioinformatics *26*, 841–842.

Rada-Iglesias, A., Bajpai, R., Swigut, T., Brugmann, S.A., Flynn, R.A., and Wysocka, J. (2011). A unique chromatin signature uncovers early developmental enhancers in humans. Nature *470*, 279–283.

Robinson, M.D., McCarthy, D.J., and Smyth, G.K. (2010). edgeR: A Bioconductor package for differential expression analysis of digital gene expression data. Bioinformatics *26*, 139–140.

Russo, M.W., Sevetson, B.R., and Milbrandt, J. (1995). Identification of NAB1, a repressor of NGFI-A- and Krox20-mediated transcription. Proc. Natl. Acad. Sci. USA *92*, 6873–6877.

Schaukowitch, K., Joo, J.Y., Liu, X., Watts, J.K., Martinez, C., and Kim, T.K. (2014). Enhancer RNA facilitates NELF release from immediate early genes. Mol. Cell *56*, 29–42.

Scott, E.W., Simon, M.C., Anastasi, J., and Singh, H. (1994). Requirement of transcription factor PU.1 in the development of multiple hematopoietic lineages. Science *265*, 1573–1577.

Stadelmayer, B., Micas, G., Gamot, A., Martin, P., Malirat, N., Koval, S., Raffel, R., Sobhian, B., Severac, D., Rialle, S., et al. (2014). Integrator complex regulates NELF-mediated RNA polymerase II pause/release and processivity at coding genes. Nat. Commun. *5*, 5531.

Svaren, J., Sevetson, B.R., Apel, E.D., Zimonjic, D.B., Popescu, N.C., and Milbrandt, J. (1996). NAB2, a corepressor of NGFI-A (Egr-1) and Krox20, is induced by proliferative and differentiative stimuli. Mol. Cell. Biol. *16*, 3545–3553.

Thierion, E., Le Men, J., Collombet, S., Hernandez, C., Coulpier, F., Torbey, P., Thomas-Chollier, M., Noordermeer, D., Charnay, P., and Gilardi-Hebenstreit, P. (2017). Krox20 hindbrain regulation incorporates multiple modes of cooperation between cis-acting elements. PLoS Genet. *13*, e1006903.

van den Berg, D.L.C., Azzarelli, R., Oishi, K., Martynoga, B., Urbán, N., Dekkers, D.H.W., Demmers, J.A., and Guillemot, F. (2017). Nipbl interacts with Zfp609 and the integrator complex to regulate cortical neuron migration. Neuron *93*, 348–361.

Whyte, W.A., Orlando, D.A., Hnisz, D., Abraham, B.J., Lin, C.Y., Kagey, M.H., Rahl, P.B., Lee, T.I., and Young, R.A. (2013). Master transcription factors and mediator establish super-enhancers at key cell identity genes. Cell *153*, 307–319.

Wickham, H. (2009). Ggplot2: Elegant Graphics for Data Analysis. (Springer).

Younesy, H., Nielsen, C.B., Lorincz, M.C., Jones, S.J., Karimi, M.M., and Möller, T. (2016). ChAsE: Chromatin analysis and exploration tool. Bioinformatics *32*, 3324–3326.

Zentner, G.E., Tesar, P.J., and Scacheri, P.C. (2011). Epigenetic signatures distinguish multiple classes of enhancers with distinct cellular functions. Genome Res. *21*, 1273–1283.

Zhan, X., and Liu, D.J. (2015). SEQMINER: An R-Package to Facilitate the Functional Interpretation of Sequence-Based Associations. Genet. Epidemiol. *39*, 619–623.

Zhang, Y., Liu, T., Meyer, C.A., Eeckhoute, J., Johnson, D.S., Bernstein, B.E., Nusbaum, C., Myers, R.M., Brown, M., Li, W., and Liu, X.S. (2008). Model-based analysis of ChIP-seq (MACS). Genome Biol. *9*, R137.

STAR★METHODS

KEY RESOURCES TABLE

REAGENT or RESOURCE	SOURCE	IDENTIFIER
Antibodies		
Rabbit polyclonal anti-Asunder	Bethyl	Cat#A303-575A
Rabbit polyclonal anti-EGR1	Bethyl	Cat#A303-390A
Mouse monoclonal anti-EGR1	Santa Cruz Biotechnology	Cat#sc-515830
Rabbit polyclonal anti-EGR2	Abiocode	Cat#R0814-3
Rabbit polyclonal anti-INTS1	Bethyl	Cat#A300-361A
Rabbit polyclonal anti-INTS11	Bethyl	Cat#A301-274A
Mouse monoclonal anti-INTS6	Santa Cruz Biotechnology	Cat#sc-376524
Mouse monoclonal anti-NAB2	Santa Cruz Biotechnology	Cat#sc-23867
Rabbit polyclonal anti-NAB2	ThermoFisher	Cat#PA5-27925
Rabbit monoclonal anti-GAPDH	Cell Signaling Technology	Cat#2118
Mouse monoclonal anti-γ-tubulin	Santa Cruz Biotechnology	Cat#sc-17788
Mouse monoclonal anti- α-tubulin	Sigma-Aldrich	Cat#T9026
Rabbit polyclonal anti-H3K27ac	Abcam	Cat# ab4279
Rabbit polyclonal anti-H3K4me1	Abcam	Cat# ab8895
Rabbit polyclonal anti-PolII	This paper	See STAR Methods
Normal rabbit IgG	Santa Cruz Biotechnology	Cat# sc-2027
PE-Cy7 anti-mouse/human CD11b	BioLegend	Cat#101215
APC anti-human CD11b	BD Biosciences	Cat#550019
PE anti-human CD14	BD Biosciences	Cat#561707
FITC anti-human CD34	BD Biosciences	Cat#560942
APC anti-human CD33	BD Biosciences	Cat#561817
Anti-rabbit IgG (HRP)	Cell Signaling Technology	Cat#7074
Anti-mouse IgG (HRP)	Cell Signaling Technology	Cat#7076
Biological Samples		
De-identified human cord blood	Helen F. Graham Cancer Center and Research Institute, Christiana Hospital	
Chemicals, Peptides, and Recombinant Proteins		
StemSpan SFEM medium	STEMCELL Technologies	Cat# 09650
StemSpan CC100, cytokine cocktail	STEMCELL Technologies	Cat# 02690
Phorbol 12-myristate 13-acetate (PMA)	Sigma-Aldrich	Cat#P8139
FcR blocking reagent, human	Myltenyi Biotec	Cat#130-059-901
Recombinant human SCF	Peprotech	Cat#300-07
Recombinant human IL-3	Peprotech	Cat#200-03
Recombinant human M-CSF	Peprotech	Cat#300-25
Recombinant human GM-CSF	Peprotech	Cat#300-03
Recombinant human IL-6	Peprotech	Cat#200-06
Recombinant human FLT3L	Peprotech	Cat#300-19
MethoCult SF H4236, methylcellulose medium	STEMCELL Technologies	Cat#04236
Dynabeads protein A	Invitrogen	Cat#10002D
protein A – HRP conjugated	Cell Signaling Technologies	Cat#12291
Anti-FLAG M2 affinity gel	Sigma-Aldrich	Cat#A2220
FLAG peptide	Sigma-Aldrich	Cat#F3290

(*Continued on next page*)

Continued

REAGENT or RESOURCE	SOURCE	IDENTIFIER
Critical Commercial Assays		
CD34 MicroBeads kit, human	Miltenyi Biotec	Cat#130-046-702
Gibson Assembly Master Mix	New England Biolabs	Cat#E2611S
Phusion High-fidelity DNA polymerase kit	New England Biolabs	Cat#M0530S
Direct-zol RNA Miniprep kit	Zymo research	Cat#R2051
Revertaid first strand cDNA synthesis kit	Thermo Scientific	Cat#K1622
Cell growth determination kit MTT based	Sigma-Aldrich	Cat# CGD1
ChIP DNA Clean & Concentrator kit	Zymo research	Cat#D5201
NEBNext Ultra II DNA Library Prep Kit for Illumina	New England Biolabs	Cat#E7645S
NEBNext Multiplex Oligos for Illumina (Index Primers set 1)	New England Biolabs	Cat#E7335S
NEBNext rRNA depletion kit	New England Biolabs	Cat#E6310L
NEBNext Ultra Directional RNA Library Prep kit	New England Biolabs	Cat#E7420S
miRNeasy mini kit	QIAGEN	Cat#217004
Deposited Data		
ChIP-seq data	This paper	GEO: GSE106359
RNA-seq data	This paper	GEO: GSE106359
Chromatin RNA-seq	This paper	GEO: GSE106359
Experimental Models: Cell Lines		
Human: 293T cells	ATCC	Cat# CRL-3216
Human: HL-60 cells	ATCC	Cat# CCL-240
Human: Bone marrow derived CD34+ cells	Calabretta Lab	N/A
Human: Fetal liver derived CD34+ cells	Stem Cell and Xenograft Core, University of Pennsylvania	https://www.med.upenn.edu/cores/stem_cell_and_xenograft.html
Monocytes	Human Immunology Core, University of Pennsylvania	https://pathbio.med.upenn.edu/hic/site/
Oligonucleotides		
Primers (see Table S3)	This paper	N/A
shRNA sequences (See Table S3)	This paper	N/A
Recombinant DNA		
pLKO.1	Addgene	Cat#10879
Tet-pLKO-puro	Addgene	Cat#21915
pLENTI-CMV-GFP-Puro	Addgene	Cat#17448
pLKO.1-shINTS11 #1	Sigma-Aldrich	TRCN0000161507
pLKO.1-shINTS11 #2	Sigma-Aldrich	TRCN0000161070
pLKO.1-shNAB2 #1	Sigma-Aldrich	TRCN0000019544
pLKO.1-shNAB2 #3	Sigma-Aldrich	TRCN0000019546
pLKO.1-shINTS13 #1	This paper	N/A
pLKO.1-shINTS13 #2	This paper	N/A
Tet-pLKO-shEGR1	This paper	N/A
pLKO.1-shNAB2 #2	This paper	N/A
pLENTI-FLAG-NAB2	This paper	N/A
Software and Algorithms		
FlowJo Software v10.0.7	FlowJo, LCC	
MaxQuant v1.5.2.8	Cox and Mann, 2008	
STAR v2.5	Dobin et al., 2013	
Samtools v0.1.19	Li et al., 2009	
FeatureCounts	Liao et al., 2014	

(*Continued on next page*)

Continued

REAGENT or RESOURCE	SOURCE	IDENTIFIER
RSEM	Li and Dewey, 2011	
DESeq2	Love et al., 2014	
BWA tool	Li, 2013	
MACS2	Zhang et al., 2008	
ChAsE v1.0.11	Younesy et al., 2016	
EdgeR	Robinson et al., 2010	
Ggplot package	Wickham, 2009	
BEDtools v2.25.0	Quinlan and Hall, 2010	
SeqMINER v1.3.4	Zhan and Liu, 2015	
Other		
Superose 6 10/30 GL column	GE Life Science	Cat# 17517201

CONTACT FOR REAGENT AND RESOURCE SHARING

Further information and requests for resources and reagents should be directed to and will be fulfilled by the Lead Contact, Alessandro Gardini (agardini@wistar.org)

EXPERIMENTAL MODEL AND SUBJECT DETAILS

Cell lines

293T were obtained from American Type Culture Collection (ATCC) and maintained in Dulbecco's Modified Eagle's Medium (DMEM) supplemented with 10% super calf serum (GEMcell) and 2 mM L-glutamine (Corning). HL-60 cells were obtained from ATCC and maintained in Roswell Park Memorial Institute (RPMI)-1640 medium (Corning) supplemented with 10% (v/v) of super calf serum (GEMcell) or Tet system approved fetal bovine serum (Clontech) and 2 mM of L-glutamine (Corning). Jurkat cells were a kind gift of Dr. M. Abdel-Mohsen (Wistar Institute).

Primary cells

Bone marrow (BM)-derived CD34+ were obtained from Calabretta's lab at Thomas Jefferson University. CD34+ CD33- cells were sorted at the Flow Cytometry facility at Wistar Institute. Fetal liver (FL)-derived CD34+ cells were obtained from Stem Cell and Xenograft Core at University of Pennsylvania and were maintained in StemSpan SFEM medium supplemented with CC100 cytokine cocktail (Stem Cell Technologies). De-identified human cord blood (CB) was obtained from volunteers with informed consent at Helen F. Graham Cancer Center and Research Institute at Christiana Hospital. Mononucleated cells (MNC) were separated with Ficoll-Hystopaque Plus (GE Healthcare). CD34+ cells were then isolated using human CD34 MicroBeads Kit (Miltenyi Biotec) following manufacturer's instructions. CD34+ were maintained in StemSpan SFEM medium supplemented with 1X CC100 cytokine cocktail. BM- and FL-derived CD34+ were used for CFU assay, BM-, FL- and CB-derived CD34+ were *in vitro* differentiated and used for RNA-seq and ChIP-seq experiments, respectively. Circulating monocytes were obtained from the Human Immunology Core at University of Pennsylvania.

METHOD DETAILS

Lentiviral infection

HL-60 cells were lentivirally transduced through one round of spinoculation (1800 RPM, 45 minutes at 30°C, brake off) and selected with 2 μg/ml puromycin (InvivoGen). CD34+ cells were spinoculated with ultracentrifuge-concentrated lentivirus at 1800 RPM, for 45 minutes at 30°C, incubated overnight at 37°C in the virus-containing medium, followed by another round of infection the following day. Cells were collected, washed and selected with 1 μg/ml puromycin in StemSpan SFEM medium supplemented with CC100 cytokine cocktail (Stem Cells Technologies).

In vitro differentiation

HL-60 cells were differentiated with 100 nM Phorbol 12-myristate 13-acetate (PMA) in growing medium and the status of differentiation was assessed by flow cytometry. Briefly, cells were incubated in 1X PBS supplemented with 1% heat-inactivated FBS and 2 mM EDTA with FcR blocking reagent (1:20 dilution, Miltenyi Biotech) for 30 minutes at 4°C, washed with 1X PBS and incubated

with the suitable fluorochrome-conjugated antibody for 30 minutes at 4°C. Cells were then washed with 1X PBS, fixed in 1% formaldehyde (Sigma-Aldrich) in 1X PBS. Cells were then washed twice with cold PBS and data acquired with a BD LSR II flow cytometer (BD Bioscience). Analyses were performed and elaborated using FlowJo Software v10.0.7 (FlowJo, LLC).

CD34+ cells were differentiated in monocytes in SFEM supplemented with 100 ng/ml SCF, 10 ng/ml IL-3, 50 ng/ml M-SCF and 25 ng/ml GM-CSF (Peprotech). Expression of CD14 was assessed by flow cytometry at different days of treatment as a measure of differentiation (CD14+ cells: day 0: 0%–4%, day 3: 3%–7%, day 7: 20%–40%). Circulating monocytes were differentiated into adherent macrophages in IMDM supplemented with 10% heat-inactivated FBS and 25 ng/ml of human recombinant GM-CSF (Peprotech).

Knockdown of INTS11, INTS13, EGR1 and NAB2

pLKO.1, tet-pLKO-puro and pLENTI-CMV-GFP-Puro vectors were obtained from Addgene (#10879, #21915 and #17448). pLKO.1-shINTS11 #1 (TRCN0000161507), pLKO.1-shINTS11 #2 (TRCN0000161070), pLKO.1-shNAB2 #1 (TRCN0000019544) and pLKO.1-shNAB2 #3 (TRCN0000019546) were obtained from the Molecular Screening Facility at the Wistar Institute. A shRNA against luciferase was used as control.

shINTS13#1, shINTS13#2, shEGR1, shNAB2 #2 were designed with the Broad Institute algorithm (https://portals.broadinstitute.org/gpp/public/) and subsequently cloned in either pLKO.1 or tet-pLKO vectors. Sequences of the designed shRNAs are listed in Table S3. Expression of tet-pLKO-shEGR1 was induced with 2 μg/ml doxycycline (Sigma-Aldrich) for 72 hours in growing medium.

NAB2 overexpression

To generate the pLENTI-FLAG-NAB2 vector, NAB2 full-length cDNA was amplified by PCR using the Phusion high-fidelity DNA polymerase kit (New England Biolabs), cloned into the pFLAG-puro vector and sub-cloned into the pLENTI-CMV-GFP-Puro using Gibson Assembly Master Mix (New England Biolabs). Primer sequences are listed in Table S3.

Western blot

Cells were harvested and washed three times in 1X PBS and lysed in RIPA buffer (50 mM Tris-HCl pH 7.5, 150 mM NaCl, 1% Igepal, 0.5% sodium deoxycholate, 0.1% SDS, 500 μM DTT) supplemented with 1 μg/ml aprotinin, 1 μg/ml leupeptin (Sigma) and 1 μg/ml pepstatin (BMB). 50 μg of whole cell lysate were loaded in Bolt 4%–12% Bis-Tris Plus gel (Invitrogen) or Novex WedgeWell 10% Tris-Glycine Gel (Invitrogen) and separated through gel electrophoresis (SDS-PAGE) in Bolt MES running buffer (Invitrogen) or Tris-Glycine-SDS buffer (Bio-Rad), respectively. Separated proteins were transferred to ImmunBlot PVDF membranes (BioRad) for antibody probing. Membranes were incubated with 10% BSA in TBST for 30 minutes at room temperature, then incubated for 2h at RT or overnight at 4°C with the suitable antibodies diluted in 5% BSA in 1X TBST, washed with TBST, and incubated with a dilution of 1:10000 of HRP-linked anti-mouse or anti-rabbit secondary antibody (Cell Signaling) for one hour at RT. Antibodies were then visualized using Clarity Western ECL substrate (Biorad) and imaged with Fujifilm LAS-3000 Imager (Fujifilm).

Real-time quantitative polymerase chain reaction

Cells were lysed in Tri-reagent and RNA was extracted using the Direct-zol RNA MiniPrep kit (Zymo research). 1 μg of template RNA was retrotranscribed into cDNA using random primers and the Revertaid first strand cDNA synthesis kit (Thermo Scientific) according to manufacturer directions. 50 ng of the cDNA were used for each real-time quantitative PCR reaction with 0.4 μM of each primer, 10 μL of iQ SYBR Green Supermix (BioRAD) in a final volume of 20 μl, using a CFX96 real-time system (BioRAD). Thermal cycling parameters were: 3 minutes at 95°C, followed by 40 cycles of 10 s at 95°C, 20 s at 63°C followed by 30 s at 72°C. Each sample was run in triplicate. *18S* rRNA weas used as normalizer. Primer sequences are reported in Table S3.

Colony-forming unit (CFU) assays

Infected FL- or BM- derived CD34+ cells were cultured at 37°C at the density of 1.2×10^3/ml in SF H4236 methylcellulose (Stem Cell Biotechnologies) containing medium supplemented with 15% heat-inactivated fetal bovine serum (Sigma-Aldrich) or 15% of super calf serum (GEMcell), 100 ng/ml SCF, 20 ng/ml IL-3, 50 ng/ml FLT3L, 20 ng/ml IL-6, 50 ng/ml M-CSF, 30 ng/ml GM-CSF. Colonies were counted after 10-14 days. Colonies were stained overnight in a solution of 5 mg/ml of Nitrotetrazolium Blue chloride (Sigma-Aldrich) in water.

Proliferation assay

HL-60 or CD34+ cells were seeded at 20,000 cells/ml in 96-well plates at day 1. Cell proliferation was determined every 24h (HL-60) or 4 days later (CD34+ cells) using the cell growth determination kit MTT based (Sigma-Aldrich), following manufacturer's instruction.

Immunoprecipitation

HL-60 cells were washed twice with ice cold PBS before resuspension in BC100 (20mM Tris pH 8.0, 0.1M KCl, 0.1% NP-40, 10% glycerol, 0.2mM EDTA, 0.5mM DTT, 1 μg/ml each of protease inhibitors aprotinin, leupeptin, and pepstatin), and incubated at 4°C for

five minutes. The pellet was resuspended in buffer C (20mM Tris pH 8.0, 1.5mM $MgCl_2$, 0.42M NaCl, 25% glycerol, 0.2mM EDTA, 0.5mM DTT, protease inhibitors) and incubated at 4°C for 30 minutes. For chromatin-enriched nuclear extracts, Benzonase nuclease (Sigma-Aldrich) was added after 15 minutes and incubated for an additional 30 minutes at 4°C. The resulting extract was spun down at 12,000rpm for 30 minutes. The pellet was discarded and supernatant kept as nuclear extract. The nuclear extract was dialyzed overnight in BC80 (20mM Tris pH 8.0, 80mM KCl, 0.2mM EDTA, 10% glycerol, 1mM β-mercaptoethanol, 0.2mM phenylmethylsulfonyl fluoride (PMSF)), cleared and stored at −80°C.

500 μg (for western blot) or 2-4 mg (for mass spectrometry) of nuclear extract was diluted in co-IP buffer (20mM Tris pH 7.9, 100mM NaCl, 0.1% NP-40, protease inhibitors). INTS13 antibody-crosslinked Dynabeads Protein A (Invitrogen), or ANTI-FLAG M2 affinity gel (Sigma-Aldrich) were incubated with nuclear extract at 4°C for four or two hours, respectively. Supernatant kept as flow-through. Beads were washed three times with co-IP buffer, followed by one wash with 0.05% NP-40 in PBS. Glycine elution was performed with agitation in 0.1M glycine pH 3.0 for one minute, and 1M Tris base pH 11.0 was added to neutralize the pH of the eluate. Flag-peptide competition elution was performed by incubation with excess FLAG peptide (Sigma-Aldrich) at 4°C for 30 minutes. Eluate was stored at −80°C or prepared for SDS-PAGE.

Size-exclusion chromatography

0.4 mL of HL-60 nuclear extract (5mg total protein) was loaded onto a Superose 6 10/30 GL column (GE Life Science) equilibrated with BC500 buffer. Flow rate was fixed at 0.4 ml/min, and 0.4 mL fractions were collected.

Antibody crosslinking

Dynabeads Protein A (Invitrogen), 500 μl, were washed three times with PBS prior to crosslinking with 20 μg INTS13 antibody (Bethyl). Beads and antibody were diluted in PBST and incubated with agitation for 2 hours at room temperature. The antibody-bound beads were washed three times with 200mM triethanolamine pH 8.2, then resuspended in freshly made 10mM DMP (dimethyl pimedlimidate dihydrochloride) in 200mM triethanolamine pH 8.2 and gently rotated for 30 minutes at room temperature. The crosslinking reaction was stopped with gentle rotation in 50mM Tris pH 7.5 for 15 minutes. Crosslinked beads were washed three times with PBST, twice with 0.1M glycine pH 3.0, twice with PBST, and stored in PBST + 0.02% sodium azide at 4°C.

Mass spectrometry

After co-immunoprecipitation, eluates were prepared for SDS-PAGE as described previously. The eluates were run into a 10% Tris-glycine gel at 110V for ten minutes. The gel was stained with Colloidal Blue staining kit (Invitrogen), and further processed at the proteomics facility at the Wistar Institute. Briefly, the gel lanes were excised, digested with trypsin, and analyzed by LC-MS/MS on the Q Exactive HF mass spectrometer. The data were searched against the UniProt human database (September 2016) and provided sequences using MaxQuant 1.5.2.8 (Cox and Mann, 2008). False discovery rates for protein and peptide identifications were set at 1%.

Chromosome conformation capture (3C)

Chromosome Conformation Capture was performed as reported in (Dekker et al., 2002) with minor changes. 1×10^7 HL-60 cells were fixed in 1% formaldehyde for 10 min at room temperature for cross-linking. The reaction was quenched with 0.25 M glycine and cells were collected by centrifugation at 225 g for 8 minutes at 4°C. Cell pellet was lysed in 5 mL cold lysis buffer (10 mM Tris-HCl, pH 7.5; 10 mM NaCl; 5 mM $MgCl_2$; 0.1 mM EGTA) with freshly added protease inhibitors on ice for 10 minutes.

Isolated nuclei were collected by centrifugation at 400 g for 5 min at 4°C then re-suspended in 0.5 mL of 1X Cutsmart buffer (New England Biolabs) with 0.3% SDS and incubated for 1 h at 37°C while shaking at 900 rpm. Next, samples were incubated for 1 hr at 37°C after addition of 2% Triton X-100.

400 U of PstI restriction enzyme (New England Biolabs) were added to the nuclei and incubated at 37°C over night while shacking at 900 rpm. 5 μL of samples were collected before and after the enzyme reaction to evaluate digestion efficiency.

The reaction was stopped by addition of 1.6% SDS and incubation at 65°C for 30 minutes while shaking at 900 rpm. The sample was then diluted 10-fold with 1.15 × ligation Buffer (660 mM Tris-HCl, pH 7.5, 50 mM DTT, 50 mM $MgCl_2$, 10mM ATP) and 1% Triton X-100 and incubated for 1 h at 37°C while shaking at 900 rpm. 100 U of T4 DNA ligase (NEB) were added to the sample and the reaction was carried at 16°C over night. For each sample, 300 μg of Proteinase K were added for protein digestion and de-crosslinking at 65°C overnight. On the next day, RNA was removed by adding 300 μg of RNase and incubating the sample for 1 h at 37°C. DNA was purified twice by phenol-chloroform extraction, and precipitated with ethanol over night at −80°C. Purified DNA was quantified by qubit, diluted to 3ng/ul and analyzed by real time quantitative PCR. The ΔCt method was applied for analyzing data, using the actin Ct values as control.

Primer sequences are reported in Table S3.

ChIP-seq and ChIP-qPCR sample processing

Samples from different conditions were processed together to prevent batch effects. ChIP-seq was performed as previously described (Lai et al., 2015), with some modifications. For each replicate, 10 million HL-60 cells were cross-linked with 1%

formaldehyde for 5 min at room temperature, harvested and washed twice with 1 × PBS. The pellet was resuspended in ChIP lysis buffer (150 mM NaCl, 1% Triton X-100, 0,7% SDS, 500 μM DTT, 10 mM Tris-HCl, 5 mM EDTA) and chromatin was sheared to an average length of 200–400 bp, using a Covaris S220 Ultrasonicator. The chromatin lysate was diluted with SDS-free ChIP lysis buffer. For ChIP-seq, 10 μg of antibody (5 μg for histone modifications) was added to the 10 million lysated cells along with Protein A magnetic beads (Invitrogen) and incubated at 4°C overnight. For RNAPII ChIP-seq, a custom rabbit polyclonal antibody raised against the N-terminal domain was used. On day 2, beads were washed twice with each of the following buffers: Mixed Micelle Buffer (150 mM NaCl, 1% Triton X-100, 0.2% SDS, 20 mM Tris-HCl, 5 mM EDTA, 65% sucrose), Buffer 500 (500 mM NaCl, 1% Triton X-100, 0.1% Na deoxycholate, 25 mM HEPES, 10 mM Tris-HCl, 1 mM EDTA), LiCl/detergent wash (250 mM LiCl, 0.5% Na deoxycholate, 0.5% NP-40, 10 mM Tris-HCl, 1 mM EDTA) and a final wash was performed with 1 × TE. Finally, beads were resuspended in 1 × TE containing 1% SDS and incubated at 65°C for 10 min to elute immunocomplexes. Elution was repeated twice, and the samples were further incubated overnight at 65°C to reverse cross-linking, along with the untreated input (5% of the starting material). On day 3, after treatment with 0.5 mg/ml proteinase K for 3 h, DNA was purified with Zymo ChIP DNA Clear Concentrator kit (Zymo research) and quantified with QUBIT. Barcoded libraries were made with NEB ULTRA II DNA Library Prep Kit for Illumina, and sequenced on Illumina NextSeq 500, producing 75bp SE reads. For ChIP-qPCR samples, on day 3 DNA was purified with Wizard SV Gel and PCR Clean-Up system (Promega), resuspended in 200 ul and 5 ul were for each PCR reaction. Primer sequences are listed in Table S2

ChIP-seq analyses

Sequences were aligned to the reference hg19, using Burrows Wheeler Alignment tool (BWA), with the MEM algorithm (Li, 2013). Aligned reads were filtered based on mapping quality (MAPQ > 10) to restrict our analysis to higher quality and likely uniquely mapped reads, and PCR duplicates were removed. We called peaks for each individual using MACS2, at 5% FDR, with default parameters (Zhang et al., 2008). Heatmaps and average profiles were generated with ChAsE v. 1.0.11 (Younesy et al., 2016). EdgeR (Robinson et al., 2010) was used to detect cis-regulatory elements (CREs) which significantly gained INTS13 and/or INTS11 after PMA treatment (FDR < 10%). Specifically, INTS11 PMA peaks replicated across all samples were used as reference for the INTS11 differential binding analysis. Similarly, INTS13 replicated across all samples were used as reference for the INTS13 differential binding analysis.

Subcellular fractionation

Subcellular fractionation was performed as described (Lai et al., 2015), with minor changes. Briefly, cells were resuspended in cold cytoplasmic lysis buffer (10 mM Tris-HCl pH 7.5, 150 mM NaCl, 0.15% NP-40) using wide orifice tips, incubated on ice for 5 minutes, layered onto cold sucrose buffer (10 Mm Tris-HCl pH 7.5, 150 Mm NaCl, 24% sucrose w/v) and centrifuge at 13,000 rpm for 10 minutes at 4°C. Nuclei were gently resuspended in glycerol buffer (20 mM Tris pH 7.9, 75 mM NaCl, 0.5 mM EDTA, 50% glycerol, 0.85 mM DTT) using wide orifice tips, and same amount of nuclei lysis buffer (20 mM HEPES pH 7.6, 7.5 mM $MgCl_2$, 0.2 mM EDTA, 0.3 M NaCl, 1 M urea, 1% NP-40, 1 mM DTT) was added. After a brief incubation for 1 minute on ice, chromatin was isolated by centrifugation at 14,000 rpm for 2 minutes at 4°C. Chromatin-bound RNA was isolated with Trizol protocol and miRNeasy kit (QIAGEN).

RNA-seq sample processing

Samples from different conditions were processed together to prevent batch effects. Total RNA and chromatin-bound RNA were extracted using Zymo Direct-Zol RNA miniprep Kit (Zymo research) and miRNeasy kit with Trizol protocol and in-column DNase treatment (QIAGEN), respectively. Quality of total RNA was assessed by the RNA Integrity Number (RIN) using Agilent Bioanalyzer. All retained RNA samples had a RIN > 8.

1 μg of total or chromatin-bound RNA were depleted of ribosomal RNA using the NEBNext rRNA depletion kit (New England Biolabs). rRNA-depleted RNA was purified with the miRNEasy kit (QIAGEN) and used to produce barcoded RNA sequencing libraries using the NEBNext Ultra Directional RNA Library Prep kit (New England Biolabs), and sequenced on Illumina NextSeq 500, producing 75bp SE reads.

RNA-seq analyses

Reads were aligned to hg19 using STAR v2.5 (Dobin et al., 2013), in 2-pass mode with the following parameters:–quantMode TranscriptomeSAM–outFilterMultimapNmax 10–outFilterMismatchNmax 10–outFilterMismatchNoverLmax 0.3–alignIntronMin 21–alignIntronMax 0–alignMatesGapMax 0–alignSJoverhangMin 5–runThreadN 12–twopassMode Basic–twopass1readsN 60000000–sjdbOverhang 100. We filtered bam files based on alignment quality (q = 10) using Samtools v0.1.19 (Li et al., 2009). We used the latest annotations obtained from Ensembl to build reference indexes for the STAR alignment. FeatureCounts (Liao et al., 2014) was used to count reads mapping to each gene. RSEM (Li and Dewey, 2011) was instead used to obtain FPKM (Fragments Per Kilobase of exon per Million fragments mapped). We analyzed differential gene expression levels using read counts, normalized by feature length with DESeq2 (Love et al., 2014), with the following model: design = ~condition, where condition indicates either CTRL or PMA.

QUANTIFICATION AND STATISTICAL ANALYSIS

All statistical analyses were performed using R v3.3.1.

DATA AND SOFTWARE AVAILABILITY

The accession number for the total RNA-seq, chromatin RNA-seq and ChIP-seq data reported in this paper is GEO: GSE106359.

Figures were made with the package ggplot2 (Wickham, 2009). BEDtools v2.25.0 (Quinlan and Hall, 2010) was used for genomic analyses.